PATENT
3722-0170P

IN THE U.S. PATENT AND TRADEMARK OFFICE

Applicant:	CHOU, Bruce C.S.	Conf.:
Appl. No.:	New	Group:
Filed:	November 24, 2003	Examiner:
For:	THERMAL BUBBLE TYPE MICRO INERTIAL SENSOR	

L E T T E R

Commissioner for Patents
P.O. Box 1450
Alexandria, VA 22313-1450

November 24, 2003

Sir:

Under the provisions of 35 U.S.C. § 119 and 37 C.F.R. § 1.55(a), the applicant(s) hereby claim(s) the right of priority based on the following application(s):

Country	Application No.	Filed
TAIWAN	091134748	November 29, 2002

A certified copy of the above-noted application(s) is(are) attached hereto.

If necessary, the Commissioner is hereby authorized in this, concurrent, and future replies, to charge payment or credit any overpayment to Deposit Account No. 02-2448 for any additional fee required under 37 C.F.R. §§ 1.16 or 1.17; particularly, extension of time fees.

Respectfully submitted,

BIRCH, STEWART, KOLASCH & BIRCH, LLP

By _____
Joe McKinney Muncy, #32,334

P.O. Box 747
Falls Church, VA 22040-0747
(703) 205-8000

KM/cqc
3722-0170P

Attachment(s)

(Rev. 09/30/03)

BSNB 703-205-8000
Chou
3722-0170P
Nov. 24, 2003
1071

中華民國經濟部智慧財產局

INTELLECTUAL PROPERTY OFFICE
MINISTRY OF ECONOMIC AFFAIRS
REPUBLIC OF CHINA

茲證明所附文件，係本局存檔中原申請案的副本，正確無訛，
其申請資料如下 ：

This is to certify that annexed is a true copy from the records of this office of the application as originally filed which is identified hereunder：

申　　請　　日 ： 西元 2002 年 11 月 29 日
Application Date

申　請　案　號 ： 091134748
Application No.

申　　請　　人 ： 祥群科技股份有限公司
Applicant(s)

局　　長
Director General

蔡練生

發文日期： 西元 2003 年 9 月 10 日
Issue Date

發文字號： 09220916270
Serial No.

申請日期：	IPC分類
申請案號：	

（以上各欄由本局填註）

發明專利說明書

一、發明名稱	中 文	熱泡式微型慣性感測元
	英 文	
二、發明人（共1人）	姓 名（中文）	1. 周正三
	姓 名（英文）	1.
	國 籍（中英文）	1. 中華民國 TW
	住居所（中 文）	1. 新竹市建中一路27號11樓之1
	住居所（英 文）	1.
三、申請人（共1人）	名稱或姓 名（中文）	1. 祥群科技股份有限公司
	名稱或姓 名（英文）	1.
	國 籍（中英文）	1. 中華民國 TW
	住居所（營業所）（中 文）	1. 新竹科學園區力行六路一號四樓　（本地址與前向貴局申請者相同）
	住居所（營業所）（英 文）	1.
	代表人（中文）	1. 郭維武
	代表人（英文）	1.

四、中文發明摘要　（發明名稱：熱泡式微型慣性感測元）

本發明提供一種熱泡式微型慣性感測元，係為一以微加工技術形成之微型裝置，其係在一基板上設置一加熱器，且在加熱器之四周對稱設有四組溫度感測元，以感測加熱器周圍的溫度變化，在基板上設有一封蓋，且其係包覆加熱器及該等溫度感測元以密封之，使一液相流體填充於封蓋與基板形成之空間內；利用該加熱器加熱液相流體，使之汽化形成一熱汽泡於該液相流體環境中，藉由水的表面張力及溫度控制可以控制汽泡的大小，以使加熱器四周的溫度感測元感測到溫度分布之變化，以作為一傾斜計以感測傾斜的方向及大小，亦可作為一加速規以量測加速度的方向及大小。本創作具有無質量塊、反應速度快、靈敏度高、體積小等優點。

（一）、本案代表圖為：第二圖

（二）、本案代表圖之元件代表符號簡單說明：

陸、英文發明摘要　（發明名稱：）

四、中文發明摘要 -(發明名稱：熱泡式微型慣性感測元)

1 熱泡式微慣性感測元	10 基板
12 加熱器	14、16 溫度感測元
18 封蓋	20 液相流體
22 汽泡	22a、22b、22c 等溫線

陸、英文發明摘要 (發明名稱：)

一、本案已向

國家(地區)申請專利	申請日期	案號	主張專利法第二十四條第一項優先權

二、□主張專利法第二十五條之一第一項優先權:

申請案號:

日期:

三、主張本案係符合專利法第二十條第一項□第一款但書或□第二款但書規定之期間

日期:

四、□有關微生物已寄存於國外:

寄存國家:

寄存機構:

寄存日期:

寄存號碼:

□有關微生物已寄存於國內(本局所指定之寄存機構):

寄存機構:

寄存日期:

寄存號碼:

□熟習該項技術者易於獲得,不須寄存。

五、發明說明（1）

熱泡式微型慣性感測元

（一）、【發明所屬之技術領域】

本發明係有關一種微型慣性感測元，特別是關於一種熱汽泡式的微慣性感測元，以作為傾斜計及加速規，用以感測位置、傾斜角度及加速度之變化。

（二）、【先前技術】

按，習知之慣性感測元如加速規及陀螺儀，其係作為導航控制不可或缺的元件，然而，由於其體積龐大且價格昂貴，所以不適合推廣。微機電技術為近年來興起之一種微加工技術（Micromachining Technology），利用此技術來製作微慣性感測元，特別是微加速規（Micro-accelerometer），其特性可比傳統加工技術製造者更佳、靈敏度更高，所感測之微重力加速度可達μg等級，且微加速規又具有體積輕薄短小、適合大量製造、價格便宜等優點，極適合推廣至汽車、遊戲搖桿及3-D滑鼠等消費性電子產品。其相關文獻請參閱Yazdi等人所發表之"Micromachined Inertial Sensors"（參附件一）。

在習知技術上，微加速規大部份為固態感測元，其結構通常具有一可移動之彈性質量塊及支撐該質量塊的至少一彈性支腳，習知製造技術相當多，主要係利用矽微加工技術發展者，包括以多晶矽面型微加工技術（Poly-silicon Surface Micromachining）發展者，如美國專利編號US6223598B1、US5487305、US5417111、

US5565625、US5817942及US5665915等；或以SOI(Silicon on Insulator)面型微加工技術發展者，如美國專利編號US6294400B1、US5495761、US5747353及US5447067等。然，此種結構最大缺點為彈性質量塊易受突發的外力撞擊而破壞。

為此，遂發展出一種氣體熱對流式加速規，以克服上述之缺點，其係利用氣體熱對流的自然原理取代上述質量塊之移動作用，如美國專利編號US2445394、US2554512、US3241374及US5581034，而藉由微加工技術形成氣體熱對流式加速規者請參見美國專利US5719333 及US6171880；此種方法雖然可以克服質量塊易被破壞的問題，然而，由於氣體之熱傳特性較慢，使得此種氣體熱對流式加速規的反應速度都相當慢（~30Hz），而限制了其應用，同時由於其封裝方式需要完全氣密，以控制環境壓力值，因此在實施上亦加重了成本。

有鑑於此，本發明係針對上述之種種問題，提出一種新的感測機制，藉由一熱泡式微型慣性感測元作為一傾斜計或加速規，以同時達到無質量塊及快速反應的優點。

（三）、【發明內容】

本發明之主要目的，係在提供一種熱泡式微型慣性感測元，其係利用熱傳導良好、分子密度較緻密的液相流體與高溫形成的熱汽泡間形成有相當清楚的界面之特性，作為傾斜計及加速規，以感測位置、傾斜角度及加速度之變

五、發明說明 (3)

化，具有無質量塊之優點及反應速度快之功效，以有效改善習知缺點。

本發明之另一目的，係在提出一種利用矽微加工技術形成懸浮於基板上的加熱器及溫度感測元結構，以提高加熱器的加熱效率及溫度感測元的靈敏度，進而有效提高微型慣性感測元之量測精確度。

本發明之再一目的，係在提供一種熱泡式微型慣性感測元，其係藉由微加工技術整合相關電路於單一晶片上，不但可降低成本，且兼具有體積小之優點。

為達到上述之目的，本發明一熱泡式微型慣性感測元係藉由微加工技術在一基板上設置一加熱器，在加熱器之周圍且位於該基板上分別對稱設置有至少二溫度感測元，以感測加熱器周圍的溫度變化；一封蓋設於基板上且包覆該加熱器及該等溫度感測元以密封之，使一液相流體填充於該封蓋與該基板形成之空間內。

底下藉由具體實施例配合所附的圖式詳加說明，當更容易瞭解本發明之目的、技術內容、特點及其所達成之功效。

(四)、【實施方式】

本發明之熱泡式微慣性感測元作為加速規及傾斜計之作用原理係可透過第一圖至第四圖的原理說明加以了解。首先，請參見第一圖，其係為本發明之熱泡式微慣性感測元的結構剖視圖，如圖所示，一熱泡式微慣性感測元1包

括一基板10，其通常為矽基板；在基板10上設有一加熱器12，在基板10上且位於加熱器12二側周圍對稱設置有一溫度感測元14及16，藉以感測加熱器12周圍的溫度變化，加熱器12及溫度感測元14、16之材料通常為白金或鎢等金屬，亦可為積體電路製程中常見之單晶矽或多晶矽材料，當加熱器12沒有進行加熱時，溫度感測元14、16係沒有量測到任何溫度變量的；在基板10上方並設有一封蓋18，且其係包覆加熱器12及溫度感測元14、16以密封之，另有一液相流體20填充在封蓋18與基板10形成之空間內，使加熱器12及溫度感測元14、16係處於一液相流體環境中，該液相流體20在此為高純度去離子水。

當熱泡式微慣性感測元1運作時，加熱器12會進行加熱而使其周圍溫度上升，當加熱器12溫度高於水的沸點時，位於加熱器12上方的水會部份由液相變成水蒸汽，且隨著溫度的提升，水蒸汽泡會逐漸長大。此一汽泡的形成方式類似於熱泡式噴墨印表機的驅動原理，差別者為不需要提供過多的能量於該水蒸汽泡使之爆衝脫離加熱器。在本發明中，藉由水的表面張力及溫度控制，可以控制汽泡的大小，進而控制熱泡式微慣性感測元1的靈敏度及固定其位置。

如第二圖所示，在所形成的高溫汽泡22內，其實為一具有連續式溫度梯度分布之汽泡，其具有如圖中所示之等溫線22a、22b及22c，其中，越接近加熱器12處的溫度越高，而與液相流體20形成界面交接的等溫線，其溫度為該

流體的沸點，以水為例，其溫度為100°C。當熱泡式微慣性感測元1沒有受到外力改變其慣性時，位於加熱器12二側的溫度感測元14及16係偵測到相同的溫度變化A及B（在第二圖中以圓圈大小表示溫度變化之大小）。

請參見第三圖所示，其係為本發明熱泡式微慣性感測元1藉由熱汽泡原理作為傾斜計的原理說明。當熱泡式微慣性感測元1傾斜一角度θ時，汽泡22的重力方向Z會自然的與垂直於熱泡式微慣性感測元1的法線方向N形成同一角度θ，使得溫度感測元16偵測到較大的溫度變化C，而其所對應的溫度感測元14則偵測到較小的溫度變化D，透過比較C與D則可校正傾斜的方向及大小。

再參見第四圖所示，其係為本發明熱泡式微慣性感測元1藉由熱汽泡原理作為加速規的原理說明。當熱泡式微慣性感測元1受到線性加速度時，汽泡22周圍高密度D的液相流體20會產生慣性力推擠該低密度d的汽泡22，使之受力平移，因此造成溫度感測元14感測之溫度變化E大於溫度感測元16感測的溫度變化F，透過比較E與F則可以判別並校正加速度的方向及大小。由於本發明利用熱傳導良好、分子密度較緻密的液相流體特性，以及液相流體與高溫形成的熱汽泡間具有相當清楚的界面，是故在反應速度上可以有效的克服氣體熱對流式加速規反應速度慢的缺點(~30Hz)，可以達到100Hz甚至更高。

為了提高加熱器12的加熱效率及溫度感測元14、16的靈敏度，本發明更進一步可利用矽微加工技術來形成上述

之加熱器12及溫度感測元14、16結構，特別是藉由CMOS製程及其後續的微加工方法以形成具有懸浮結構的加熱器12及溫度感測元14、16，此舉最大的優點係為可以整合相關的電路於單一晶片，使體積縮小並有效降低成本。

請參見第五圖及第六圖所示，其係分別為本發明藉由CMOS製程及後段微加工技術完成之微慣性感測元的結構剖視圖及俯視圖，其中無示出液相流體20及封蓋18，由於CMOS製程為一習知技術，在此僅針對本發明使用之材料及形成方法做描述，其餘不贅述。熱泡式微慣性感測元2包括一矽基板200，其通常為晶向（100）的矽晶圓，在矽基板200上利用矽異方性蝕刻法開設有一V型凹槽210，使一加熱器220懸浮於V型凹槽210上，加熱器220係由一懸浮薄板222及其周緣向外平行該懸浮薄板222延伸之四個對稱之細長支腳224所組成，使懸浮薄板222藉由該等細長支腳224的支撐而懸浮於矽基板200之V型凹槽210上；在加熱器220四周對應X-Y軸方向等距離設置有四組完全相同的溫度感測電阻230、240、250及260，其係分別由細長支腳231、241、251、261支撐而懸浮於V型凹槽210上方。

其中，溫度感測電阻230、240、250、260即為熱敏電阻，而作為加熱器220及溫度感測電阻230、240、250、260的材料係取自於CMOS製程中的多晶矽，或是藉由矽深蝕刻技術(如感應耦合電漿蝕刻，inductively coupled plasma-reactive ion etching, ICP-RIE)搭配XeF_2等氣體蝕刻來下切去除(undercutting)部份矽基板200材料（例

如：英國STS公司有提供雙重功能的商業機台），以形成懸浮的單晶矽結構來作為加熱器220及溫度感測電阻230、240、250、260的材料。

再如第七圖所示，熱泡式微慣性感測元2藉由一橋式電路的安排係可成為一加速規或傾斜計電性量測裝置，其係使相對應之溫度感測電阻230及240(或250及260)設置於橋式電路輸出端點的兩側，並配合電阻R1及R2之設置，以藉由一差分放大器(Differential Amplifier)A1讀取其信號差值。在本發明中，係有X-Y兩個方向的量測，故需要有溫度感測電阻230、240橋式電路及溫度感測電阻250、260橋式電路兩組橋式電路的安排。

請參見第八圖及第九圖所示，其分別為本發明藉由CMOS製程及後段微加工技術完成之另一微慣性感測元實施例的結構剖視圖及俯視圖，其中同樣亦無示出液相流體20及封蓋18。此實施例熱泡式微慣性感測元3與第五圖及第六圖不同者在於溫度感測元由溫度感測電阻230、240、250、260變成熱電偶或由數個熱電偶串連而成的熱電堆310、320、330、340，每一熱電偶/熱電堆310、320、330、340緊臨加熱器220的熱接觸區350a係懸浮於V型凹槽210上，而遠離加熱器220之冷接觸區350b則是連接於矽基板200上；其中，每一熱電偶係包含有一第一熱電偶材料360及一第二熱電偶材料362，第一熱電偶材料360係為多晶矽或上述方法形成之單晶矽，而第二熱電偶材料362則為CMOS製程中的金屬連線，通常為鋁或其合金。

同樣地，熱泡式微慣性感測元3藉由適當電路的安排亦可成為一加速規或傾斜計電性量測裝置，如第十圖所示，其係為熱泡式微慣性感測元3藉由二差分放大器安排之量測裝置示意圖，位於X座標軸上的熱電偶/熱電堆310與其對應的熱電偶/熱電堆320係連接至一差分放大器A2，而Y座標軸上相對應之熱電偶/熱電堆330及340係連接至另一差分放大器A3，藉由此安排即可決定加速度或傾斜角度的大小及方向。

本發明熱泡式微慣性感測元利用熱傳導良好、分子密度較緻密的液相流體與高溫形成的熱汽泡間形成有相當清楚的界面之特性，作為傾斜計及加速規，以感測位置、傾斜角度及加速度之變化，因此具有無質量塊之優點及反應速度快之功效；另一方面，本發明利用矽微加工技術形成懸浮於基板上的加熱器及溫度感測元結構，可提高加熱器的加熱效率及溫度感測元的靈敏度，進而可有效提高微慣性感測元之量測精確度，此外，利用微加工技術能夠將相關電路整合於單一晶片上，不但可降低成本，且兼具有體積小之優點。

以上所述係藉由實施例說明本發明之特點，其目的在使熟習該技術者能瞭解本發明之內容並據以實施，而非限定本發明之專利範圍，故，凡其他未脫離本發明所揭示之精神所完成之等效修飾或修改，仍應包含在以下所述之申請專利範圍中。

（五）、【圖號說明】

1 熱泡式微慣性感測元　　10 基板

12 加熱器　　14、16 溫度感測元

18 封蓋　　20 液相流體

22 汽泡　　22a、22b、22c 等溫線

2 熱泡式微慣性感測元　　200 矽基板

210 V型凹槽　　220 加熱器

222 懸浮薄板　　224 細長支腳

230、240、250、260 溫度感測電阻

231、241、251、261 細長支腳

3 熱泡式微慣性感測元

310、320、330、340 熱電偶/熱電堆

350a 熱接觸區　　350b 冷接觸區

360 第一熱電偶材料　　362 第二熱電偶材料

第一圖為本發明之熱泡式微慣性感測元的結構剖視圖。

第二圖為本發明之熱泡式微慣性感測元形成的高溫汽泡及溫度梯度分布示意圖。

第三圖為本發明熱泡式微慣性感測元藉由熱汽泡原理作為傾斜計的原理說明示意圖。

第四圖為本發明熱泡式微慣性感測元藉由熱汽泡原理作為加速規的原理說明示意圖。

第五圖為本發明藉由微加工製程完成之微慣性感測元的結構剖視圖。

第六圖為第五圖之俯視圖。

第七圖為第五圖及第六圖之微慣性感測元藉由橋式電路安排之示意圖。

第八圖為本發明藉由微加工製程完成之微慣性感測元另一實施例的結構剖視圖。

第九圖為第八圖之俯視圖。

第十圖為第七圖及第八圖之微慣性感測元藉由差分放大器安排之量測裝置示意圖。

六、申請專利範圍

1. 一種熱泡式微型慣性感測元，包括：

一基板；

一加熱器，其係設置在該基板上；

至少二溫度感測元，其係分別對稱設置在該加熱器之周圍且位於該基板上，以感測該加熱器周圍的溫度變化；

一封蓋，設置在該基板上且包覆該加熱器及該等溫度感測元以密封之；以及

一液相流體，其係填充於該封蓋與該基板之空間內。

2. 如申請專利範圍第1項所述之熱泡式微型慣性感測元，其中，該基板係為一矽基板。

3. 如申請專利範圍第1項所述之熱泡式微型慣性感測元，其中，該加熱器之材料係選自金屬材料、多晶矽及單晶矽其中之一者。

4. 如申請專利範圍第1項所述之熱泡式微型慣性感測元，其中，該等溫度感測元之材料係選自金屬材料、多晶矽及單晶矽其中之一者。

5. 如申請專利範圍第3項或第4項所述之熱泡式微型慣性感測元，其中，該金屬材料係選自白金及鎢其中之一者。

6. 如申請專利範圍第1項所述之熱泡式微型慣性感測元，其中，該液相流體為水。

7. 如申請專利範圍第1項所述之熱泡式微型慣性感測元，其中，在該加熱器溫度高於該液相流體的沸點時，位於該加熱器上方的該液相流體會部份由液相變成氣相，而產生汽泡。

六、申請專利範圍

8. 如申請專利範圍第1項所述之熱泡式微型慣性感測元，其中，更可在該基板上開設有一凹槽，使該加熱器及該等溫度感測元係懸浮於該基板之該凹槽上方。

9. 如申請專利範圍第8項所述之熱泡式微型慣性感測元，其中，該加熱器係由一懸浮薄板及其周緣向外平行該懸浮薄板延伸之數個對稱的細長支腳所組成，且該加熱器係藉由該等細長支腳的支撐而懸浮於該基板上方。

10. 如申請專利範圍第8項所述之熱泡式微型慣性感測元，其中，該凹槽係利用異方性蝕刻法形成。

11. 如申請專利範圍第8項所述之熱泡式微型慣性感測元，其中，該溫度感測元係由至少一細長支腳支撐而懸浮於該基板上方。

12. 如申請專利範圍第1項所述之熱泡式微型慣性感測元，其中，該溫度感測元係為一熱敏電阻。

13. 如申請專利範圍第8項所述之熱泡式微型慣性感測元，其中，該溫度感測元係為一熱電偶。

14. 如申請專利範圍第8項所述之熱泡式微型慣性感測元，其中，該溫度感測元係為一由數個熱電偶串連而成的熱電堆。

15. 如申請專利範圍第13項或第14項所述之熱泡式微型慣性感測元，其中，每一該熱電偶或熱電堆鄰接於該加熱器之部位係懸浮於該基板之該凹槽上方，而另一端係連接於該基板上。

16. 如申請專利範圍第13項所述之熱泡式微型慣性感測

元，其中，該熱電偶係包含一第一熱電偶材料及一第二熱電偶材料。

17. 如申請專利範圍第16項所述之熱泡式微型慣性感測元，其中，該第一熱電偶材料係選自多晶矽及單晶矽其中之一者，而該第二熱電偶材料係為金屬連線。

18. 如申請專利範圍第1項所述之熱泡式微型慣性感測元，其係作為微加速規之應用。

19. 如申請專利範圍第1項所述之熱泡式微型慣性感測元，其係作為傾斜計之應用。

第 1/17 頁

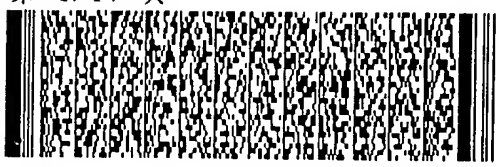

第 2/17 頁

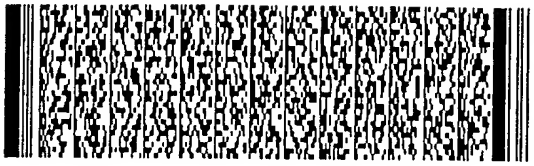

第 2/17 頁

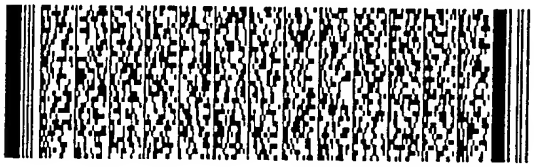

第 3/17 頁

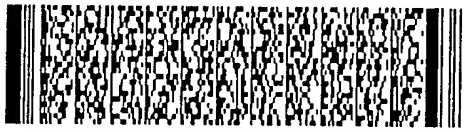

第 4/17 頁

第 5/17 頁

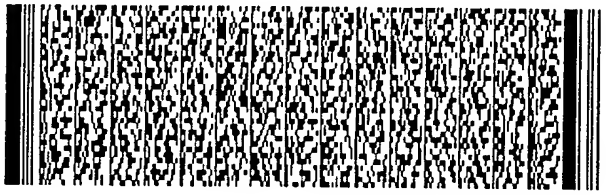

第 5/17 頁

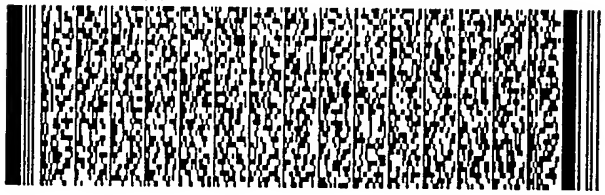

第 6/17 頁

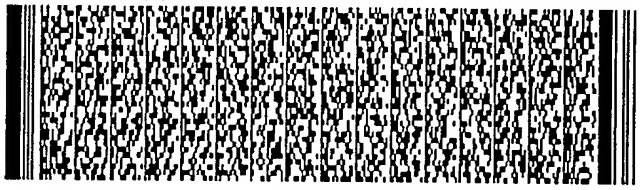

第 6/17 頁

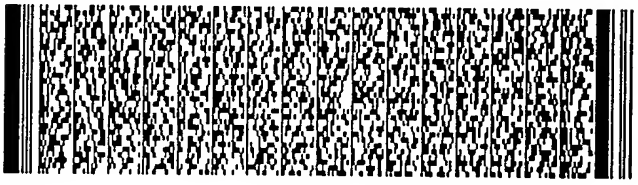

第 7/17 頁

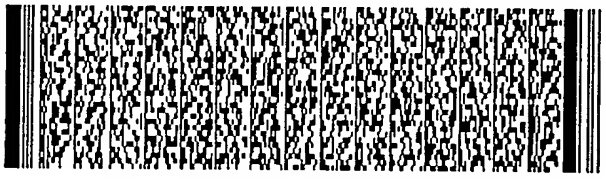

第 7/17 頁

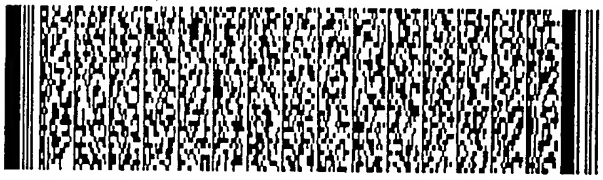

第 8/17 頁

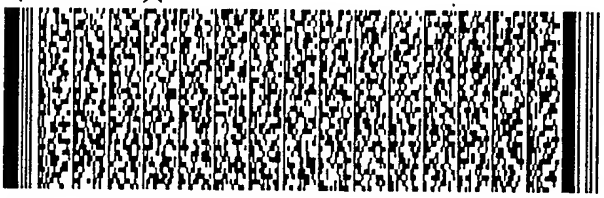

第 8/17 頁

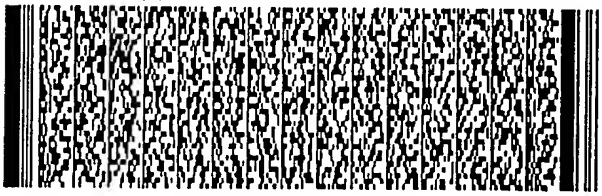

第 9/17 頁

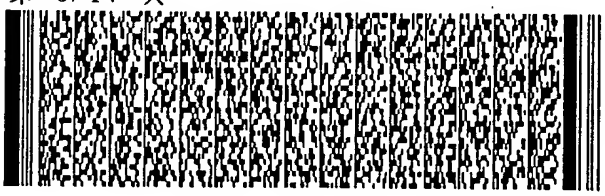

第 9/17 頁

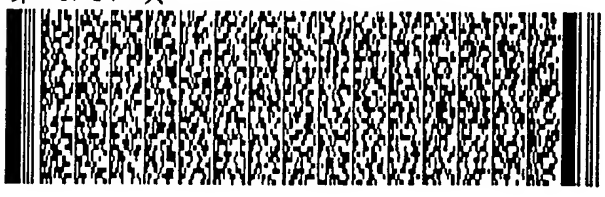

第 10/17 頁

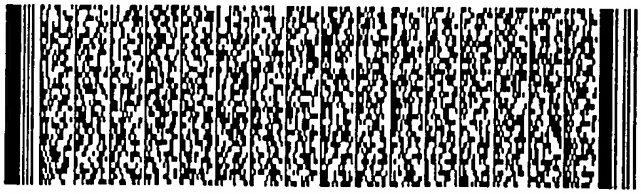

第 10/17 頁

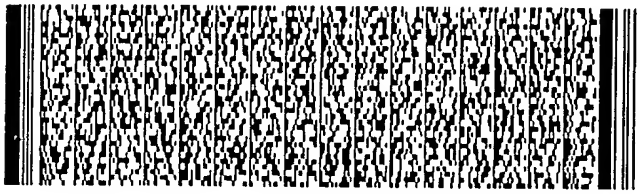

第 11/17 頁

第 11/17 頁

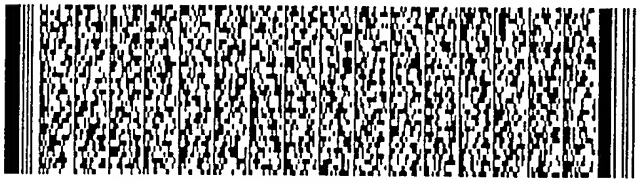

第 12/17 頁

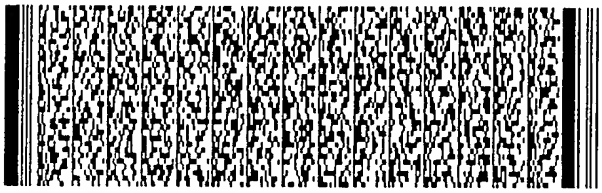

第 12/17 頁

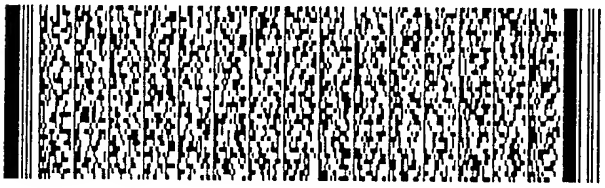

第 13/17 頁

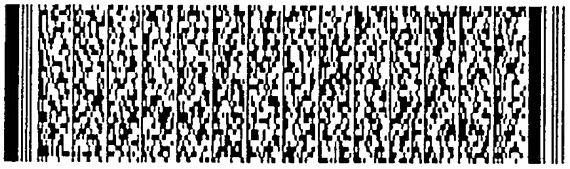

第 14/17 頁

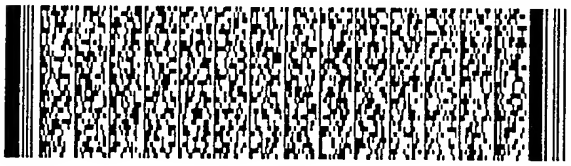

第 15/17 頁

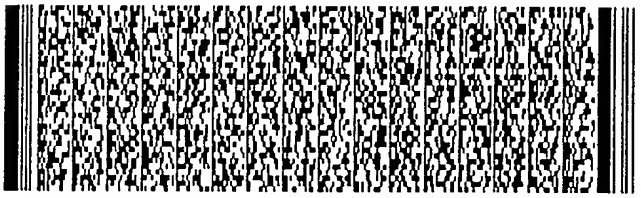

第 16/17 頁

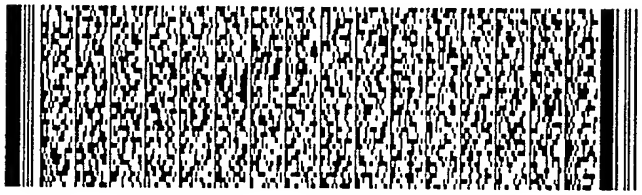

第 17/17 頁

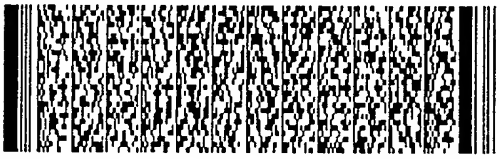

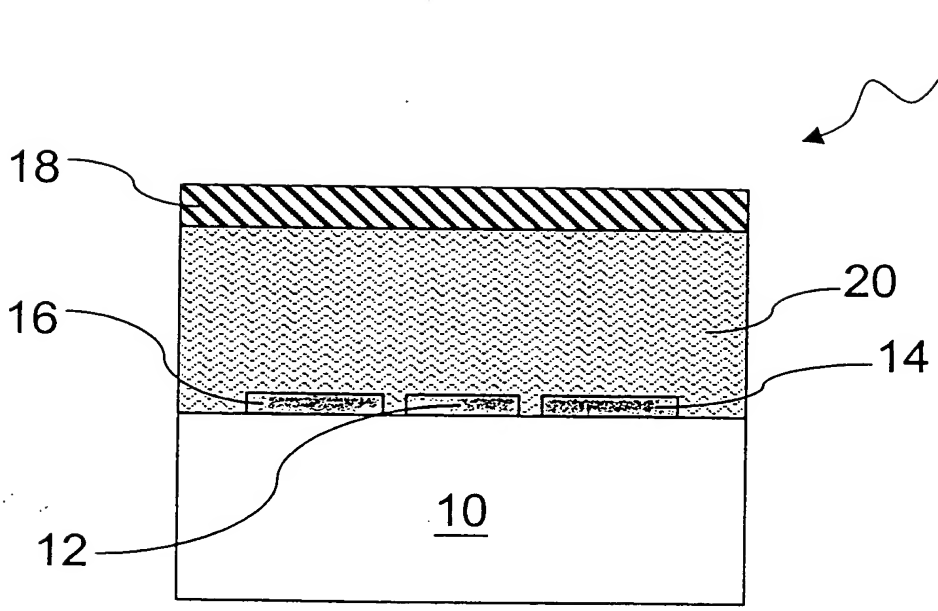

第一圖

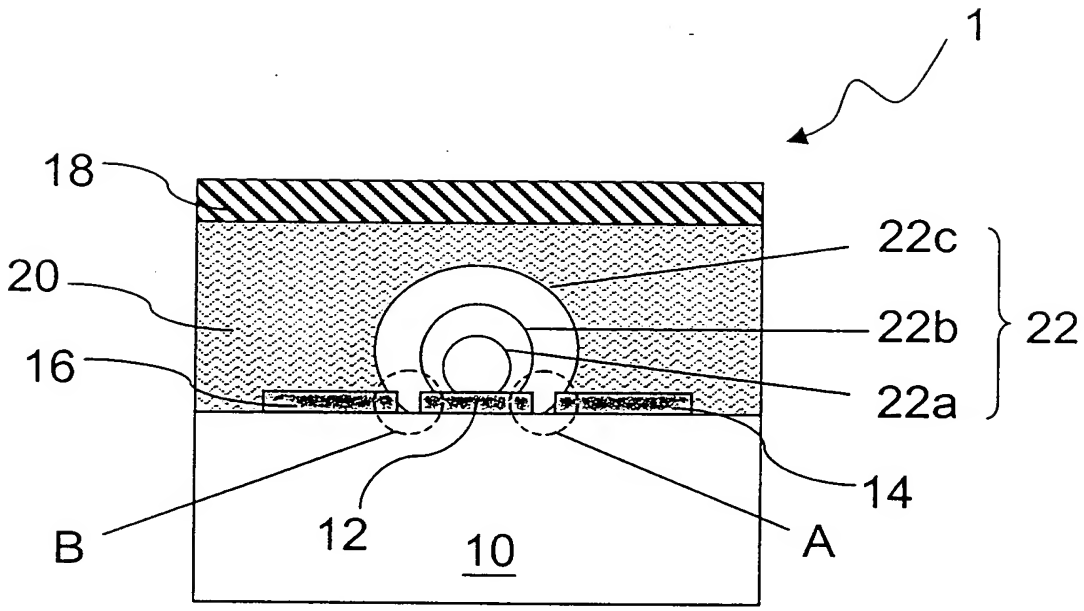

第二圖

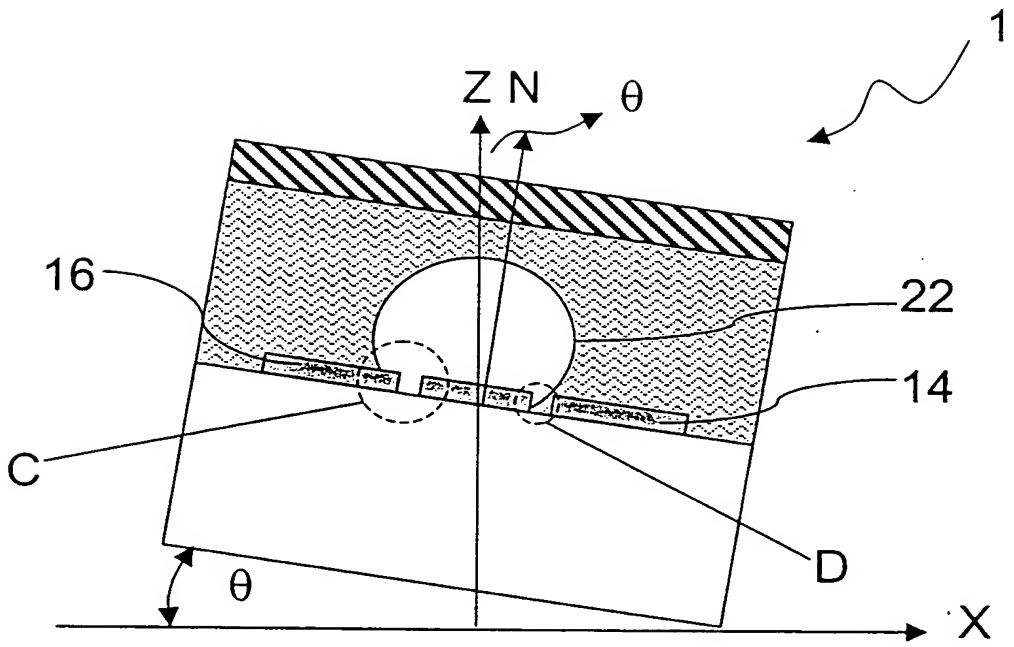

第三圖

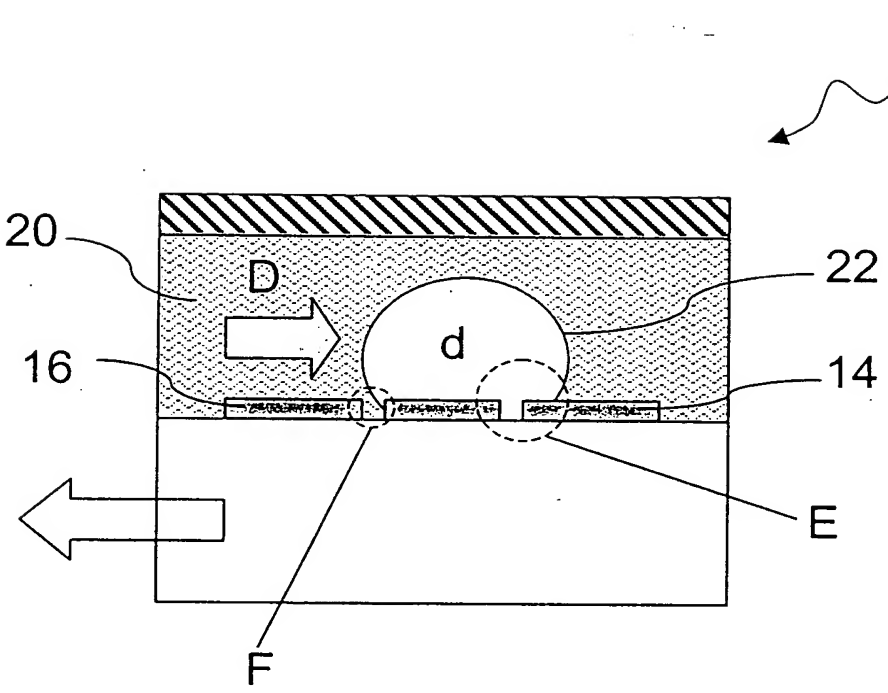

第四圖

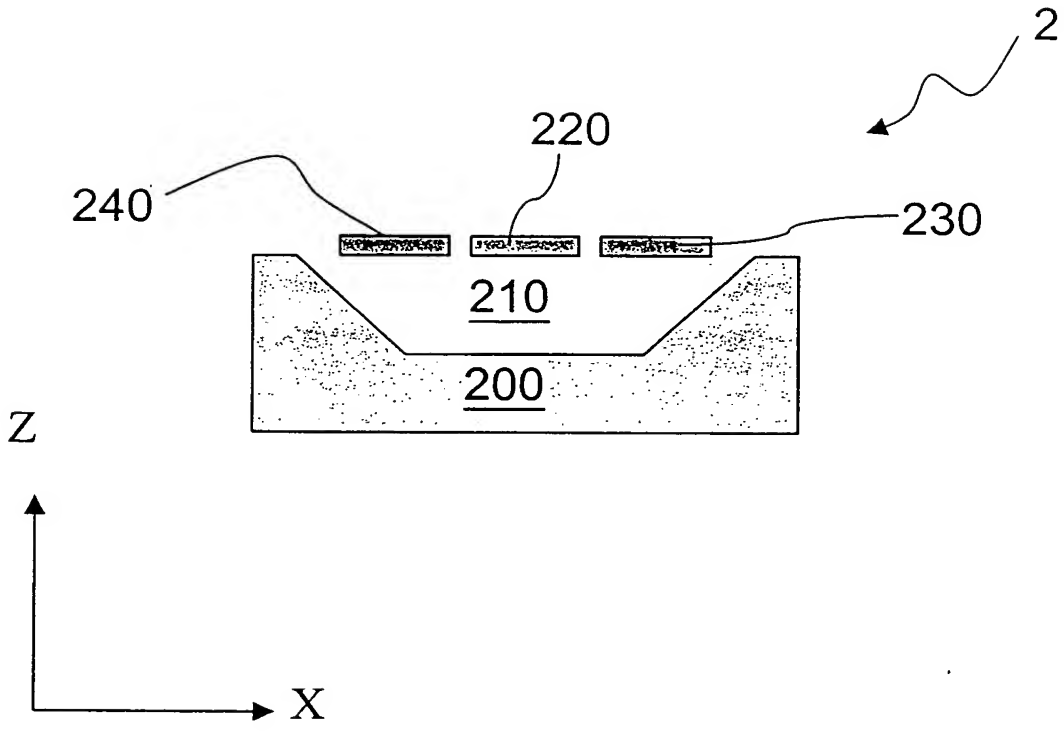

第五圖

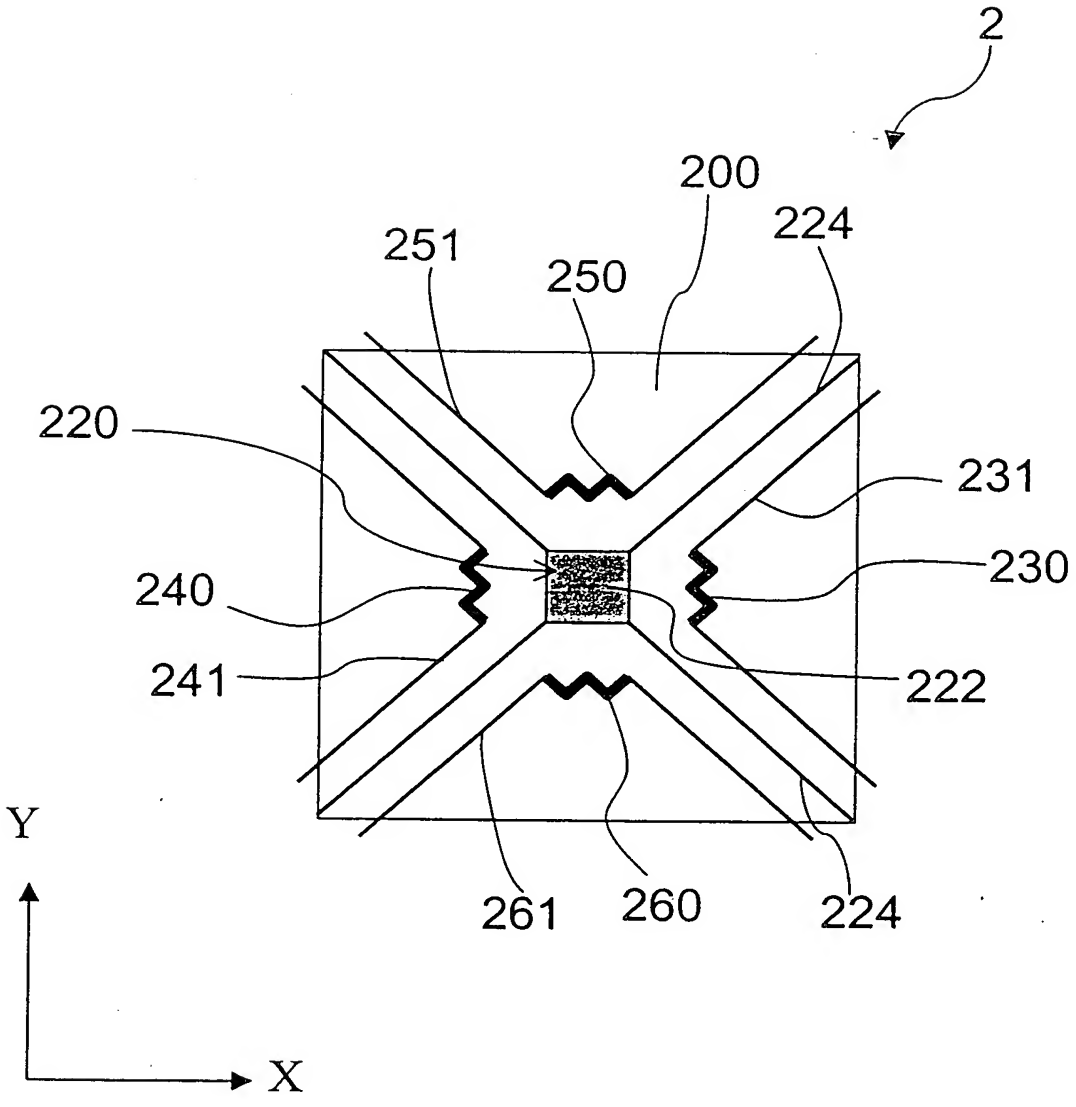

第六圖

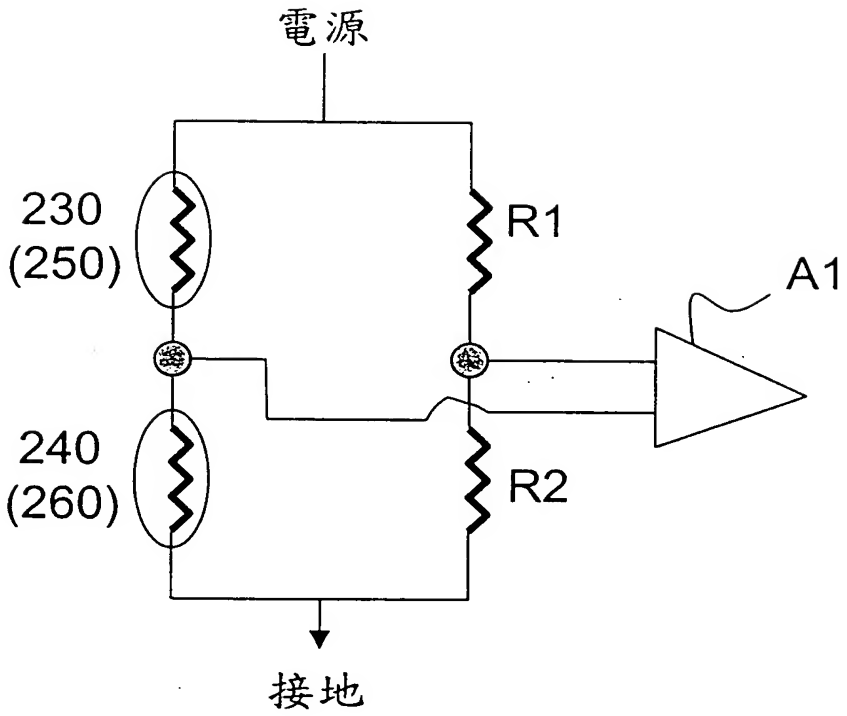

第七圖

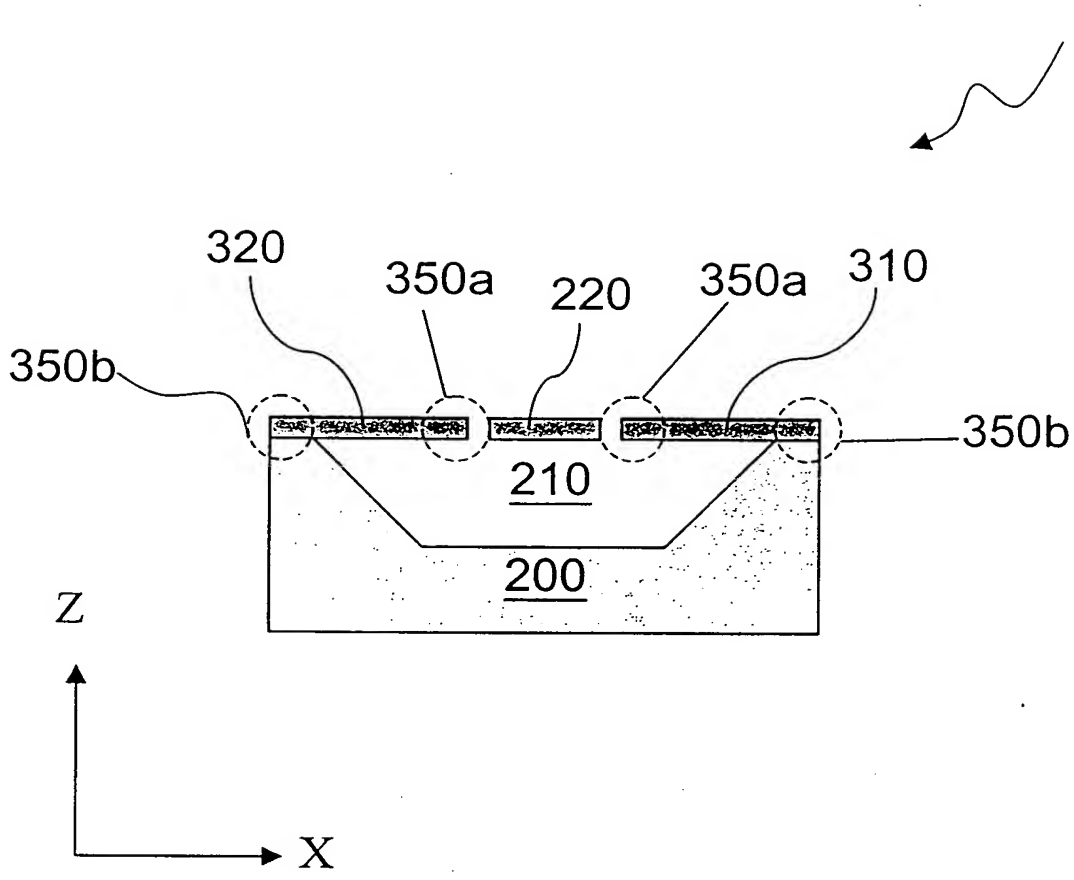

第八圖

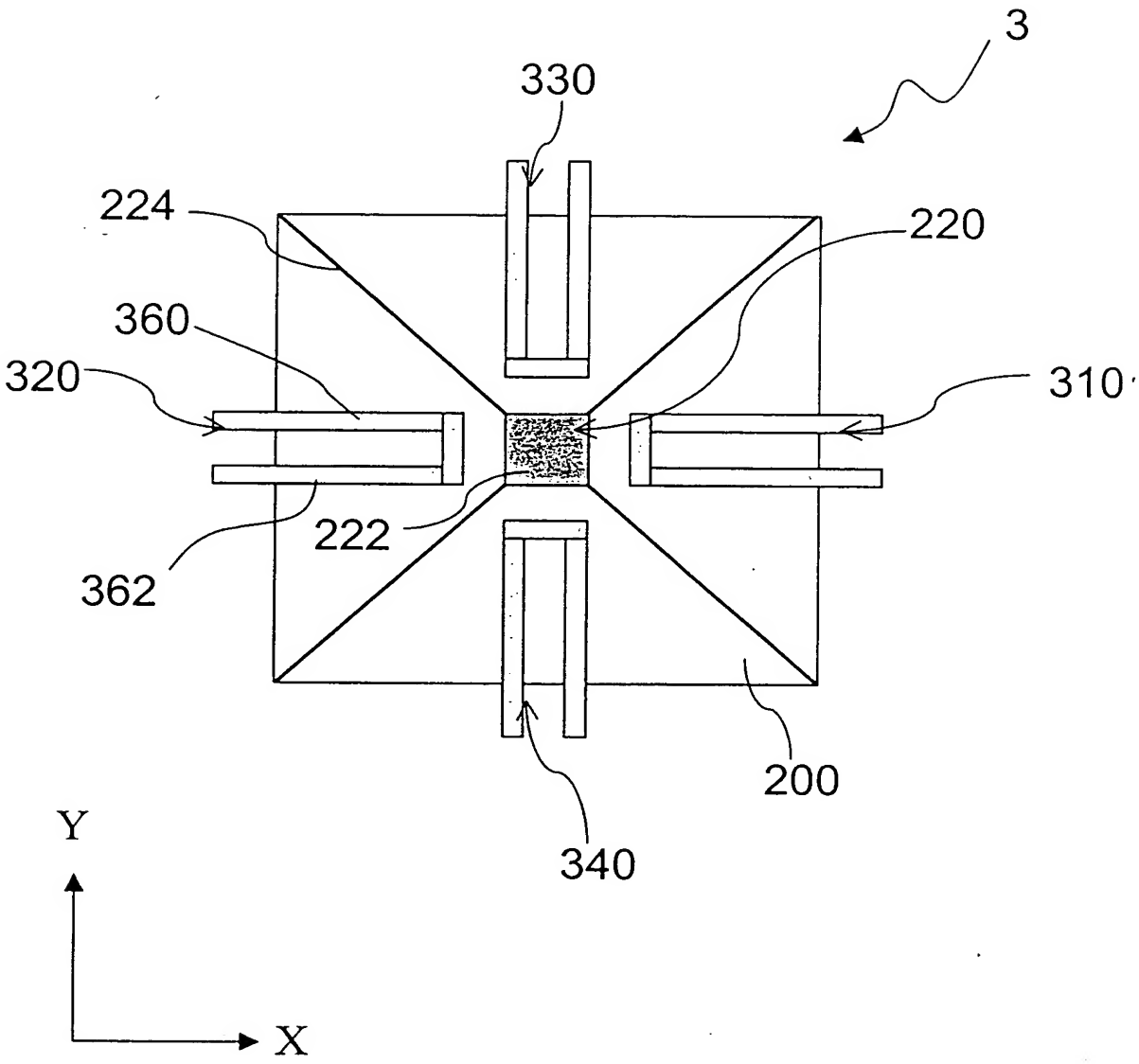

第九圖

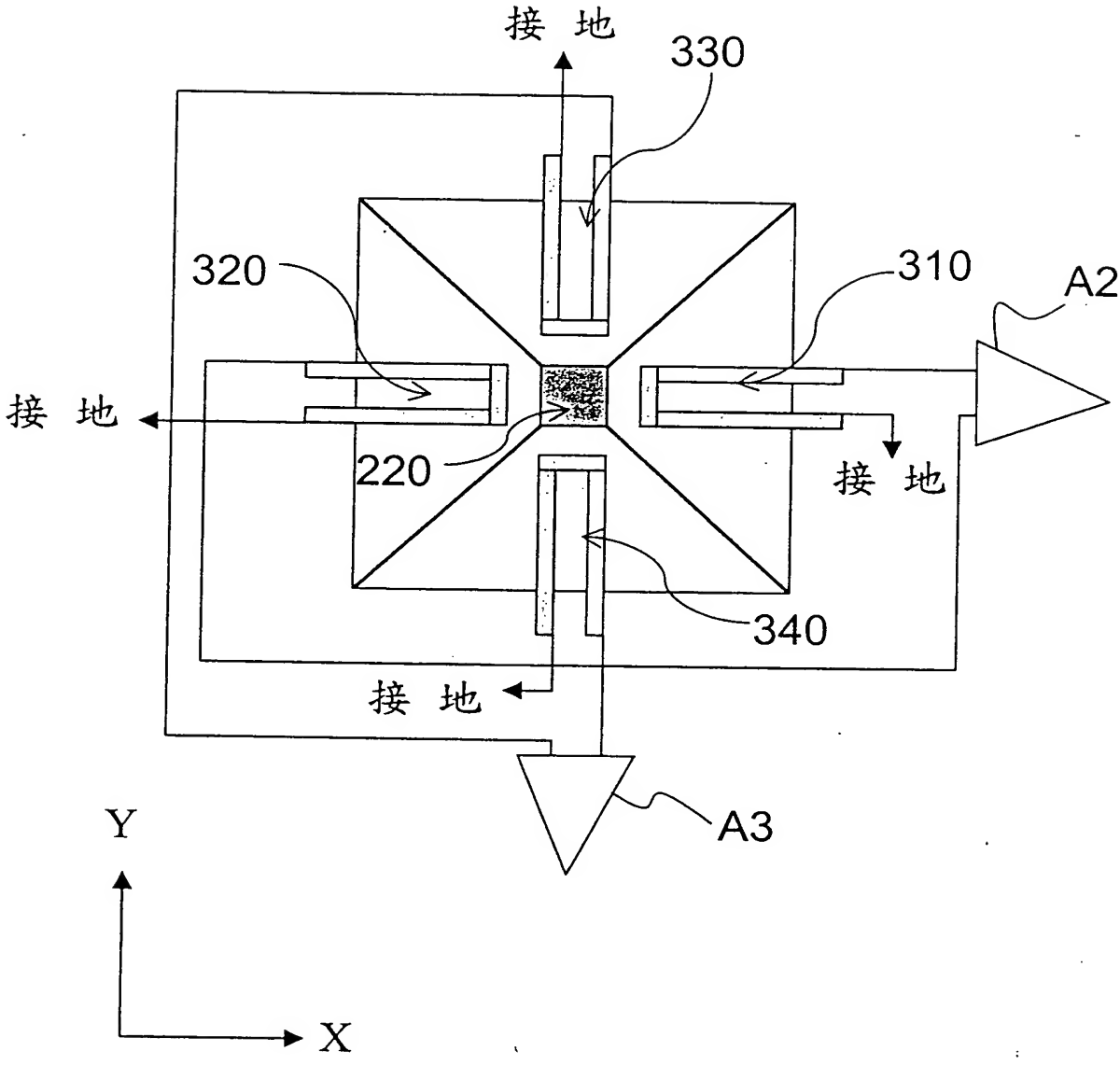

第十圖

Micromachined Inertial Sensors

NAVID YAZDI, FARROKH AYAZI, AND KHALIL NAJAFI, SENIOR MEMBER, IEEE

Invited Paper

This paper presents a review of silicon micromachined accelerometers and gyroscopes. Following a brief introduction to their operating principles and specifications, various device structures, fabrication technologies, device designs, packaging, and interface electronics issues, along with the present status in the commercialization of micromachined inertial sensors, are discussed. Inertial sensors have seen a steady improvement in their performance, and today, microaccelerometers can resolve accelerations in the micro-g range, while the performance of gyroscopes has improved by a factor of 10× every two years during the past eight years. This impressive drive to higher performance, lower cost, greater functionality, higher levels of integration, and higher volume will continue as new fabrication, circuit, and packaging techniques are developed to meet the ever increasing demand for inertial sensors.

Keywords—Accelerometer, gyroscope, inertial sensors, microfabrication technologies, micromachined sensors, micromachining, rate sensor, silicon sensors.

I. INTRODUCTION

Micromachined inertial sensors, consisting of accelerometers and gyroscopes, are one of the most important types of silicon-based sensors. Microaccelerometers alone have the second largest sales volume after pressure sensors, and it is believed that gyroscopes will soon be mass produced at similar volumes. The large volume demand for accelerometers is due to their automotive applications, where they are used to activate safety systems, including air bags, to implement vehicle stability systems and electronic suspension. However, the application of accelerometers covers a much broader spectrum where their small size and low cost have even a larger impact. They are used in biomedical applications for activity monitoring; in numerous consumer applications, such as active stabilization of picture in camcorders, head-mounted displays and virtual reality, three-dimensional mouse, and sport equipment; in industrial applications such as robotics and machine and vibration monitoring; in many other applications, such as tracking and monitoring mechanical shock and vibration during transportation and handling of a variety of equipment and goods; and in several military applications, including impact and void detection and safing and arming in missiles and other ordnance. High-sensitivity accelerometers are crucial components in self-contained navigation and guidance systems, seismometry for oil exploration and earthquake prediction, and microgravity measurements and platform stabilization in space. The impact of low-cost, small, high-performance, micromachined accelerometers in these applications is not just limited to reducing overall size, cost, and weight. It opens up new market opportunities such as personal navigators for consumer applications, or it enhances the overall accuracy and performance of the systems by making formation of large arrays of devices feasible.

Micromachined gyroscopes for measuring rate or angle of rotation have also attracted a lot of attention during the past few years for several applications. They can be used either as a low-cost miniature companion with micromachined accelerometers to provide heading information for inertial navigation purposes or in other areas [1], including automotive applications for ride stabilization and rollover detection; some consumer electronic applications, such as video-camera stabilization, virtual reality, and inertial mouse for computers; robotics applications; and a wide range of military applications. Conventional rotating wheel as well as precision fiber-optic and ring laser gyroscopes are all too expensive and too large for use in most emerging applications. Micromachining can shrink the sensor size by orders of magnitude, reduce the fabrication cost significantly, and allow the electronics to be integrated on the same silicon chip.

This paper will review both micromachined accelerometers and gyroscopes by providing an introduction to their basic operation, reviewing different types of devices reported in the literature and their performance, discussing important issues in their design and operation, and presenting a summary and conclusion along with a discussion on the future trends in this important category of micromachined

Manuscript received March 9, 1998; revised April 29, 1998. The work at the University of Michigan on inertial sensors was supported by the Defense Advanced Research Project Agency under Contracts JFBI 92-149 and DABT63-C-0111 and by the National Science Foundation under NSF-NYI Grant ECS-925-7400.

The authors are with the Center for Integrated Sensors and Circuits, Department of Electrical Engineering and Computer Science, University of Michigan, Ann Arbor, MI 48109-2122 USA.

Publisher Item Identifier S 0018-9219(98)05106-8.

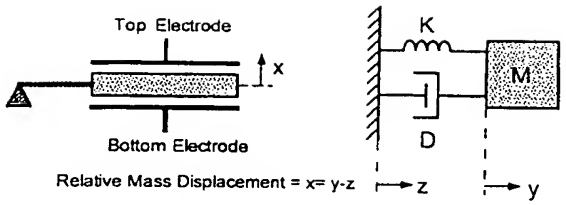

Fig. 1. General accelerometer structure and its mechanical lumped model.

sensors. Due to space constraints, interface electronics and packaging issues for inertial sensors are only briefly described. Also, other topics such as temperature compensation, calibration, and self-testing are not discussed in this paper.

II. Micromachined Accelerometers

A. Structure, Operation, and Specifications

An accelerometer generally consists of a proof mass suspended by compliant beams anchored to a fixed frame. The proof mass has a mass of M, the suspension beams have an effective spring constant of K, and there is a damping factor (D) affecting the dynamic movement of the mass. The accelerometer can be modeled by a second-order mass-damper-spring system, as shown in Fig. 1. External acceleration displaces the support frame relative to the proof mass, which in turn changes the internal stress in the suspension spring. Both this relative displacement and the suspension-beam stress can be used as a measure of the external acceleration.

By using Newton's second law and the accelerometer model, the mechanical transfer function can be obtained

$$H(s) = \frac{x(s)}{a(s)} = \frac{1}{s^2 + \frac{D}{M}s + \frac{K}{M}} = \frac{1}{s^2 + \frac{\omega_r}{Q}s + \omega_r^2} \quad (1)$$

where a is the external acceleration, x is the proof mass displacement, $\omega_r = \sqrt{K/M}$ is the natural resonance frequency, and $Q = \sqrt{KM}/D$ is the quality factor. The static sensitivity of the accelerometer is shown to be

$$\frac{x_{\text{static}}}{a} = \frac{M}{K} = \frac{1}{\omega_r^2}. \quad (2)$$

As evident, the resonance frequency of the structure can be increased by increasing the spring constant and decreasing the proof mass, while the quality factor of the device can be increased by reducing damping and by increasing proof mass and spring constant. Last, the static response of the device can be improved by reducing its resonant frequency.

The primary mechanical noise source for the device is due to Brownian motion of the gas molecules surrounding the proof mass and the Brownian motion of the proof-mass suspension or anchors. The total noise equivalent acceleration (TNEA) [$\text{m/s}^2\sqrt{\text{Hz}}$]) is [2]

$$\text{TNEA} = \frac{\sqrt{4K_BTD}}{M} = \sqrt{\frac{4K_BT\omega_r}{QM}} \quad (3)$$

where K_B is the Boltzmann constant and T is the temperature in kelvin. Equation (3) clearly shows that to reduce mechanical noise, the quality factor and proof mass have to be increased.

In the most general case, the proof-mass motion can have six degrees of freedom. But typically in a unidirectional accelerometer, the geometrical design of the suspension is such that one of these is dominant [3] and the device has low off-axis sensitivity. The cantilever support has been one of the early popular suspension support designs [4], [5] due to its simplicity, lower spring constant, and internal stress relief of the beams. However, this configuration results in a larger off-axis sensitivity unless the device is fully symmetric. Also, symmetric full-bridge supports result in a very low off-axis sensitivity [6]–[8], and by using a crab-leg or folded-beam configuration [3] in a full-bridge support, the residual stress of the beams can also be relieved. The general design of accelerometers can be performed using the above equations, as well as mechanical relations describing the spring constant [9], [10] and damping factor as a function of device geometry and ambient pressure [11], [12]. Further, the device first-order design optimization can be obtained using the same equations [4], [5], while the final accelerometer design can be simulated and optimized using commercially available finite element method or dedicated microelectromechanical systems (MEMS) software packages [13].

Accelerometers are typically specified by their sensitivity, maximum operation range, frequency response, resolution, full-scale nonlinearity, offset, off-axis sensitivity, and shock survival. Since micromachined accelerometers are used in a wide range of applications, their required specifications are also application dependent and cover a rather broad spectrum. For instance, for microgravity measurements devices with a range of operation greater than ±0.1 g, a resolution of less than 1 μg in a frequency range of zero frequency to 1 Hz are desired, while in ballistic and impact sensing applications, a range of over 10 000 g with a resolution of less than 1 g in a 50 kHz bandwidth is required. Table I summarizes typical performance parameters of accelerometers with medium resolution for automotive applications and high performance for inertial navigation applications.

B. Device Types

A variety of transduction mechanisms have been used in microaccelerometers. Some of the more relevant and useful approaches will be reviewed here.

1) Piezoresistive Devices: The first micromachined [4], and one of the first commercialized, microaccelerometers [14] were piezoresistive. These accelerometers incorporate silicon piezoresistors in their suspension beam. As the

Table 1 Typical Specifications of Accelerometers for Automotive and Inertial Navigation Applications

Parameter	*Automotive*	*Navigation*
Range	±50g (airbag) ±2g (vehicle stability system)	±1g
Frequency Range	DC- 400Hz	DC-100Hz
Resolution	<100mg (airbag) <10mg (vehicle stability system)	<4μg
Off-axis Sensitivity	<5%	<0.1%
Nonlinearity	<2%	<0.1%
Max. Shock in 1msec	>2000g	>10g
Temperature Range	-40°C to 85°C	-40°C to 80°C
TC of Offset	<60mg/°C	<50 μg/°C
TC of Sensitivity	< 900ppm/°C	±50ppm/°C

support frame moves relative to the proof mass, the suspension beams will elongate or shorten, which changes their stress profile and hence the resistivity of their embedded piezoresistors. These piezoresistors are generally placed at the edge of the support rim and proof mass, where the stress variation is maximum. Therefore, a resistive half-bridge or full bridge can be formed by employing two or four piezoresistors.

The main advantage of piezoresistive accelerometers is the simplicity of their structure and fabrication process, as well as their readout circuitry, since the resistive bridge generates a low output-impedance voltage. However, piezoresistive accelerometers have larger temperature sensitivity, and smaller overall sensitivity compared to capacitive devices, and hence a larger proof mass is preferred for them. The early development of bulk-micromachining technology, and the experience gained by several companies in the development and commercialization of piezoresistive pressure sensors, helped the initial development of piezoresistive microaccelerometers using bulk-micromachining and wafer-bonding technology [4], [14]–[18]. The device reported in [4] uses a silicon middle wafer to form the proof mass and the beams, while two glass wafer caps are bonded on top and bottom to cover the structure and provide shock stop and damping. Other devices [14], [15] use a lower bonded glass base and a silicon overhang on the top for shock stop, which is formed by silicon fusion bonding and etch back. Recently, monolithic implementation of a piezoresistive microaccelerometer with its interface complementary metal–oxide–semiconductor (CMOS) circuitry was demonstrated [17], [18], which is based on using a slight modification of a standard CMOS process to implement the accelerometer readout and temperature compensation circuitry and bulk etching of the silicon wafer from backside to form the device structure. Self-testing of the piezoresistive accelerometers is possible by using thermal actuation [15] or electrostatic forces [16]. The sensitivity of all these devices is typically around 1–2 mV/g in a 20–50-g range with an uncompensated temperature coefficient of sensitivity (TCS) of <0.2%/°C.

2) Capacitive Devices: In the presence of external acceleration, the support frame of an accelerometer moves from its rest position, thus changing the capacitance between the proof mass and a fixed conductive electrode separated from it with a narrow gap. This capacitance can be measured using electronic circuitry. Silicon capacitive accelerometers have several advantages that make them very attractive for numerous applications ranging from low-cost, large-volume automotive accelerometers [19], [20] to high-precision inertial-grade microgravity devices [21]–[26]. They have high sensitivity, good dc response and noise performance, low drift, low temperature sensitivity, low-power dissipation, and a simple structure. However, capacitive accelerometers can be susceptible to electromagnetic interference (EMI), as their sense node has high impedance. This issue can be addressed by proper packaging and by shielding the accelerometer and its interface circuit.

Some of the most widely used structures for capacitive accelerometers are vertical and lateral structures, as shown in Fig. 2. Many capacitive accelerometers utilize the vertical structure, where the proof mass is separated by a narrow air gap from a fixed plate, forming a parallel plate sense capacitance [7], [8], [20]–[27]. In these devices, the proof mass moves in the direction perpendicular to its plane (z-axis) and changes the air gap. In a lateral accelerometer, a number of moving sense fingers are attached to the proof mass, and the sense capacitance is formed between these and the fixed fingers parallel to them. The sense direction in lateral accelerometers is in the proof-mass plane (x–y directions) [19], [29]–[31]. Some designs use a "see-saw" structure, shown in Fig. 3, where a proof mass is suspended by torsional beams so that one side is heavier than the other side and in response to acceleration in the z-axis, the proof mass moves out of its plane [32]–[34]. The advantages of this structure over conventional parallel-plate z-axis devices are built-in overrange protection, larger sensitivity, and higher pull-in voltage [34].

The open-loop sensitivity of a capacitive accelerometer is proportional to the proof-mass size and capacitance overlap area and inversely proportional to the spring constant and air gap squared. Early micromachined capacitive accelerometers [7], [21]–[23] utilized bulk silicon micromachining and wafer bonding to achieve a thick, large proof mass and high sensitivity. One of the first reported devices [21] used a silicon middle wafer anodically bonded to two glass wafers on top and bottom to form a z-axis accelerometer. The device had two differential sense capacitors, with the proof mass forming the middle electrode and metal on the glass wafers forming the top/bottom fixed electrodes. The air gap was formed by recessing the silicon or glass wafers. This device with a proof-mass size of 4.6 mgr and air gap of 2 μm provided μg-level performance. The second generation of this device [22] had a resolution of better than 1 $\mu g/\sqrt{Hz}$ in a bandwidth of zero frequency to 100 Hz, with a temperature coefficient of offset (TCO) of 30 μg/°C and TCS of 150 ppm/°C. To

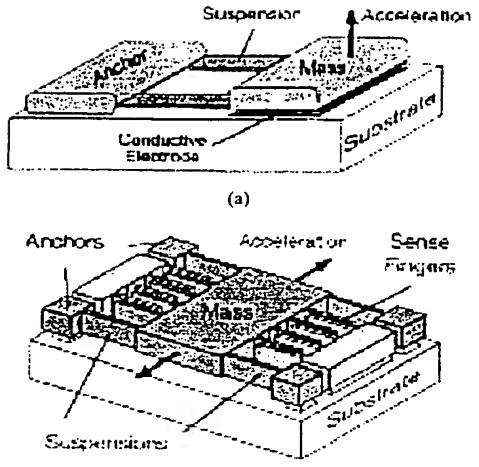

Fig. 2. Structure of (a) vertical and (b) lateral capacitive accelerometers [69].

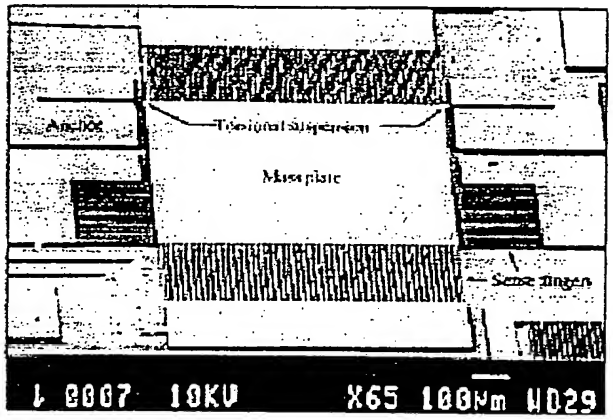

Fig. 3. A z-axis capacitive torsional accelerometer [34].

reduce its temperature sensitivity and long-term drift, the later generation of this device was fabricated using three silicon wafers [24], [35]. Another significant early design with μg performance was fabricated using glass–silicon bonding and bulk micromachining and utilized a closed-loop $\Sigma\Delta$ readout and control circuit to achieve a 120 dB dynamic range [23].

A number of capacitive microaccelerometers with medium resolution have been fabricated using the bulk silicon dissolved wafer process [27], [33], [34]. Among these, the device reported in [33] is in high-volume production by Ford. The z-axis accelerometer presented in [27] incorporates damping holes in the proof mass to control damping and uses a second silicon wafer, bonded on top, to provide overrange protection. The torsional accelerometer shown in [34, Fig. 3] is fabricated using a three-mask dissolved wafer process. It uses multiple interdigitated fingers and a varying overlap area method of capacitance change to achieve higher linearity, larger

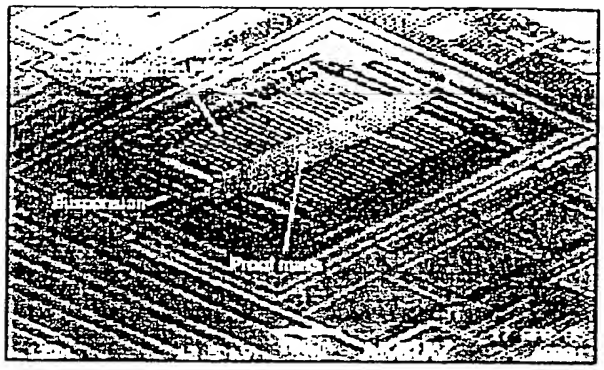

Fig. 4. SEM view of Analog Device's ADXL05 surface-micromachined polysilicon accelerometer [39].

pull-in voltage, and lower damping. The device consists of a 12-μm-thick boron-doped silicon inertial mass suspended 7.5 μm above the glass substrate by two narrow, high-aspect-ratio, 12 × 3 μm torsion beams. A large number of 300-μm-long capacitive sense fingers are attached to the end of the proof mass and are separated by a 2 μm air gap from fixed fingers anchored to the substrate. The accelerometer provides a sensitivity of 20 fF/g over a range of ±4 g and a bandwidth of 30 Hz in atmosphere.

Surface-micromachined accelerometers [19], [20], [29], [30], [36]–[40] offer the opportunity to integrate the sensor and interface circuitry on a single chip. These devices utilize deposited polysilicon layers to form the sense element and are well suited for both vertical and lateral capacitive accelerometers. Integration of the interface circuitry with the sensor enables detection of very small capacitance variation (<1aF [38]), while the accelerometer and all its interface electronics can be implemented in a small area. Fig. 4 shows a scanning electron microscope (SEM) view of the ADXL05, a polysilicon accelerometer developed and in production by Analog Devices, which has 0.5 mg/$\sqrt{\text{Hz}}$ noise floor with a range of ±5 g and shock survivability of 1000 g [39]. Also, by employing a vertical and two lateral accelerometers, an integrated three-axis accelerometry system has been designed by researchers at Berkeley and fabricated through Sandia National Laboratory's process [38]. The same group has also developed a three-axis accelerometer with a single sense element, as shown in [40], (Fig. 5). Typically, surface microaccelerometers achieve several 100 μg resolution in ~100 Hz bandwidth [37]–[40]. All of these devices have small proof mass and hence high mechanical noise (unless the device is vacuum packaged).

While bulk-micromachined devices can attain higher resolution due to their large proof mass, they generally require wafer bonding. These devices, if not formed using only silicon wafers, could have large temperature coefficients. Moreover, forming damping holes in their thick structural layers is not easy, and they typically require packaging at a specified pressure to control the damping [35]. To address these shortcomings, an all-silicon, fully symmetric,

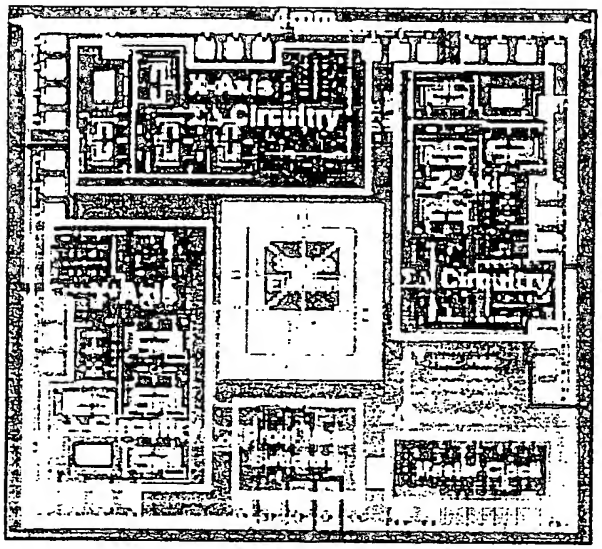

Fig. 5. Photograph of a monolithic three-axis polysilicon surface micromachined accelerometer with integrated sigma–delta readout and control circuit [40].

high-precision accelerometer has been developed [26], as shown in Fig. 6. This device uses a combined surface and bulk micromachining process to obtain a large proof mass, controllable/small damping, and a small air gap for large capacitance variation—all by using a single silicon wafer. Sense electrodes are created by depositing polysilicon on the wafer. These electrodes, while thin, are made very stiff by embedding thick vertical stiffeners (using a trench refill technology) in them so that force rebalancing of the proof mass becomes possible. There are eight suspension beams, which are symmetric with respect to the proof-mass centerline and result in low cross-axis sensitivity. An SEM view is shown in Fig. 6(b). This device is operated closed loop using an oversampled Σ/Δ modulator. It achieves a high sensitivity of 2 pF/g with a full-bridge support, a low noise level, and low temperature sensitivity, which enable it to attain μg and sub-μg performance.

3) Tunneling Devices: Some high-resolution physical sensors, including microaccelerometers [41]–[47], use a constant tunneling current between one tunneling tip (attached to a movable microstructure) and its counterelectrode to sense displacement. Fig. 7 [44] shows the general operating principal of a micromachined tunneling accelerometer. As the tip is brought sufficiently close to its counter-electrode (within a few angstroms) using electrostatic force generated by the bottom deflection electrode, a tunneling current (I_{tun}) is established and remains constant if the tunneling voltage (V_{tun}) and distance between the tip and counterelectrode are unchanged. Once the proof mass is displaced due to acceleration, the readout circuit responds to the change of current and adjusts the bottom deflection voltage V_o to move the proof mass back to its original position, thus maintaining a constant tunneling current. Acceleration can be measured by reading out the bottom deflection voltage in this closed-loop system. Tunneling accelerometers can achieve very high sensitivity with a small size since the tunneling current is highly sensitive to displacement, typically changing by a factor of two for each angstrom of displacement [48]. However, these devices have larger low-frequency noise levels [49].

Micromachined tunneling accelerometers were first introduced by researchers with the Jet Propulsion Laboratory (JPL), Pasadena, CA [41]–[43]. One of their more recent devices provides a bandwidth of several kilohertz, with a noise floor of less than 10^{-7} g/$\sqrt{\text{Hz}}$ in the 10–200-Hz frequency range [43]. However, a high supply voltage (tens to hundreds of volts) is required for these devices, thus limiting their application. Using the dissolved wafer process, a low-voltage micromachined tunneling accelerometer has been developed [44], [46], [47]. This accelerometer has a noise spectral density of the sensor-circuit module of 4 mg/$\sqrt{\text{Hz}}$ (at 0.5 Hz) and 0.1 mg/$\sqrt{\text{Hz}}$ (at 2.5 kHz) and has a minimum detectable acceleration of 8 mg in a 2.5 kHz bandwidth [47]. In continuous operation over 720 h, the accelerometer shows an offset and sensitivity variation of <0.5% [47]. Since these sensors are operated in a closed-loop mode, and since the operating current levels are typically very small, the drift of the tunneling barrier usually does not have a large impact on the performance of the sensor [46].

4) Resonant Devices: The main advantage of resonant sensors is their direct digital output. The first resonant accelerometers were fabricated using quartz micromachining [50], [51]. Silicon resonant accelerometers are generally based on transferring the proof-mass inertial force to axial force on the resonant beams and hence shifting their frequency [52]. To cancel device thermal mismatches and nonlinearities, a differential matched resonator configuration can be used [53]. Recently, two high-sensitivity resonant accelerometers have been reported [54], [55]. The devices use wafer-thick proof mass and achieve high resolution (700 Hz/g with 524 kHz center frequency [55]) and very good stability (2 μg in more than several days [54]). However, these devices typically have small bandwidth (less than a few hertz). Also recently, surface-micromachined resonant accelerometers are developed [56], [57]. The resonator reported in [57] consists of parallel beams, and its operation is based on rigidity change of the resonator due to its cross-sectional shape change, which is induced by the external acceleration. In this manner, the device is expected to achieve high sensitivity of 10%/g [57].

5) Thermal Devices: Another class of accelerometers is based on thermal transduction. One of the first thermal accelerometers used the principle that the temperature flux from a heater to a heat-sink plate is inversely proportional to their separation [58]. Hence, by measuring the temperature using thermopiles, the change in separation between the plates (which is representative of acceleration) can be measured. Devices with a moving thermopile array

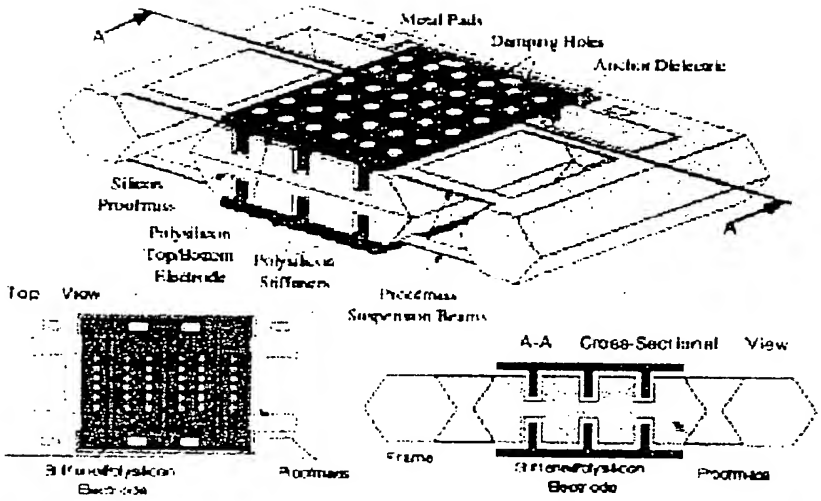

(a)

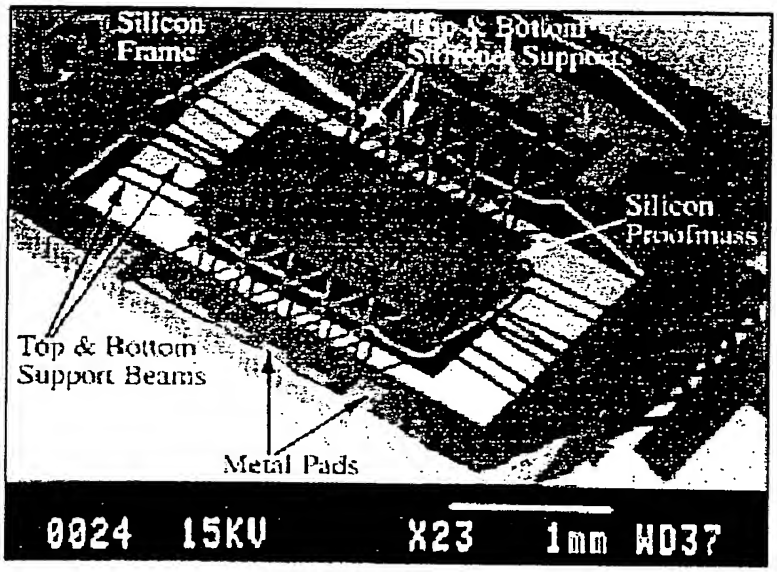

(b)

Fig. 6. (a) μg z-axis microaccelerometer structure. (b) SEM of a fabricated device [26].

and fixed heater, and vice versa, can be fabricated [58]. Recently, a novel thermal accelerometer was reported that does not have any moving mechanical parts. Its operation is based on free-convection heat transfer of a small hot air bubble in a sealed chamber [59]. The device consists of a thermally isolated heater that forms a hot air bubble. The heat distribution of this bubble changes in the presence of an acceleration and becomes asymmetric with respect to the heater. This heat profile can be sensed by two symmetrically placed temperature sensors and is a measure of the acceleration. The initial prototypes achieved a 0.6 mg sensitivity, and future devices are expected to achieve sub-μg performance [59].

6) Other Devices: In addition to the aforementioned device types, accelerometers also use many other principles, including optical [60], [61], electromagnetic [62], and piezoelectric [63], [64]. The motivation for the development of optical accelerometers has been combining optics and silicon micromachining to exploit advantages of both, as well as achieving miniature devices with very high EMI noise immunity [60] or good linearity [61]. The electromagnetic accelerometer reported in [62] utilizes two coils, one on top of the proof mass and the other separated by an air gap at the bottom, where the proof-mass displacement changes the mutual inductance of the two coils. By using a simple readout circuit with a 2.5

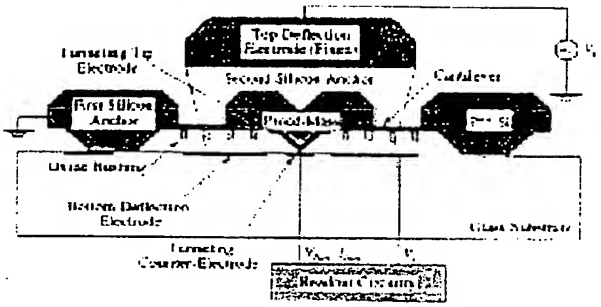

Fig. 7. Structure of a tunneling microaccelerometer [44].

mW power dissipation, a very linear response over a 50 g range was achieved [62]. Piezoelectric materials, mainly ZnO, have also been used in accelerometers to directly convert the force affecting the proof mass to an electrical signal [63], [64]. The piezoelectric charge generated by acceleration can be directly coupled to the gate of an MOS transistor and amplified [63]. One of the problems with piezoelectric materials is their leakage that deteriorates the dc response of the device. By isolating the piezoelectric film from the leakage paths, a more flat response at near dc frequencies can be obtained [63].

Also, many researchers [65]–[67] have fabricated arrays of accelerometer switches for use as a threshold or digital accelerometer. The main advantage of these devices is a digital output and simple and low-power interface circuitry [67].

In addition to bulk and surface micromachining, electroforming and mixed processes [25], [26], [28], [69] have been used to improve performance further. Electroforming can produce structures with large proof mass. For instance, a lateral accelerometer fabricated by LIGA produces a 1 $\mu g/\sqrt{Hz}$ resolution in air and a temperature-compensated TCO of 150 ppm/°C [28], [68]. The device presented in [25] uses a combination of thick epigrowth, SIMOX formation, and wafer bonding to attain high precision. The 70 μm proof mass is formed by two bonded epilayers, while the thin uniform air gap is created by etching the sacrificial buried oxide layer. A family of trench refill technologies for MEMS has been developed [69] and applied to fabricate integrated three-axis accelerometers with a medium resolution. The small mass size in surface-micromachined devices [29], [30], [36]–[40] can be somewhat circumvented by using silicon-on-insulator (SOI) wafers, where the structure height is defined by the top silicon layer, or by depositing a thick polysilicon layer using an epitaxial process [70].

C. Packaging and Interface Circuits

The accelerometer package has to protect the sensor structure without inducing significant stress or drift. Mounting errors or misalignment directly affect the sense direction of the device and its overall performance. Also, the package should not adversely affect the sensor frequency response or temperature sensitivity. Both metal can [22], [71] and multilayer ceramic hermetic packages [72] have been utilized to house the sensor and its interface circuit. The overall packaging cost can be reduced, and the performance can be improved, by packaging the sensor/circuit at the wafer level using capping glass or silicon wafers that are bonded to the device wafer, then using plastic injection molding for the final external package, as demonstrated by Motorola [73] and Ford [74].

Sensor readout and signal-processing circuit design and development is also an important aspect of micromachined accelerometers. In a piezoresistive accelerometer, the sensor piezoresistors form a half-bridge or full-bridge, and the output voltage of the bridge can be directly amplified by the interface circuit. Tunneling sensors also require simple readout circuitry that convert the tunneling current to voltage, buffer and amplify this voltage, and feed it back to the sensor [47]. Resonant sensors are operated in closed loop, and their output is their frequency, which can be measured by a digital counter. Their interface circuit consists of sense and drive circuitry. A sustaining amplifier in the loop is needed to compensate for the losses and maintain the resonance [76]. Capacitive readout circuits mostly use capacitance-to-frequency converters (oscillators) [77]–[79], capacitive ac-bridges [30], [36], or switched-capacitor circuits [24], [35], [37], [38], [80]–[82].

Accelerometers can be operated open loop or closed loop. In the open-loop mode, the overall linearity, bandwidth, and dynamic range cannot be better than the parameters of the sensor structure by itself. However, open-loop sensors require simpler interface circuitry and are inherently stable in the frequency range below their resonance.

Closed-loop operation improves the overall sensor linearity, dynamic range, and bandwidth. The interface circuitry in a closed-loop device reads the sensor signal and uses feedback to maintain the proof mass in a null position in a stable manner. Loop stability can be ensured if the accelerometer is overdamped with a dominant pole [35] or is provided using a lead compensator in the feedback path [36], or a lead-lag [23] or lead compensator [38] in the forward path. Furthermore, the dynamics of the loop can be controlled by adding an electronic pole in the loop [75]. Closed-loop accelerometers using different schemes, including phase locked loop [79], analog [82], and pulse width modulation [83], have been developed. Recently, electromechanical, oversampled, sigma–delta modulators have become more attractive, since they provide direct digital output and force-feedback control of the proof mass simultaneously over a wide dynamic range [23], [24], [33], [35]–[38].

D. Commercialization

The application of micromachined accelerometers in automotive industry has been a major driver for their initial commercialization. EG&G IC Sensors and Lucas Nova Sensors were among the first companies in the United States that commercialized mainly piezoresistive, and later capacitive, microaccelerometers [14]–[16], [31]. However, one of the most successful micromachined accelerometers

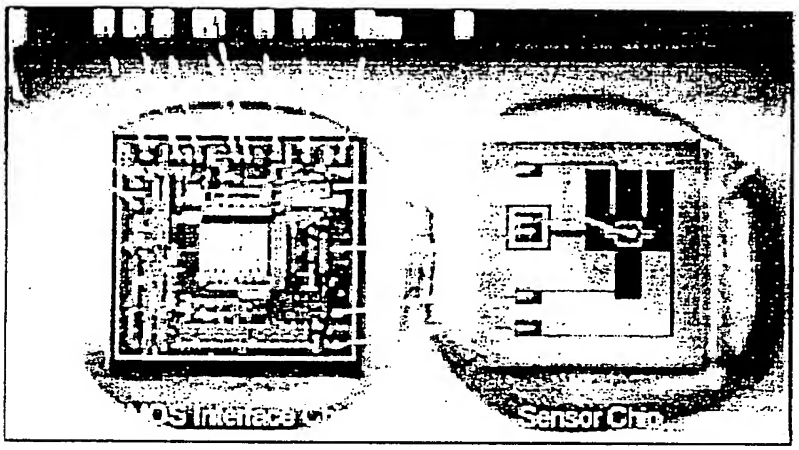

Fig. 8. Ford's accelerometer consisting of a sensor chip and a CMOS interface chip [33]. A low-cost SMD plastic package is used for this hybrid module [74].

in the market has been the ADXL50 by Analog Devices, which is a surface-micromachined, closed-loop, fully monolithic accelerometer integrated with its interface circuitry [71]. This accelerometer has been mainly developed for air-bag deployment and has a range of ±50 g with 6.6 mg/$\sqrt{\text{Hz}}$ noise floor and shock survivability of >2000 g. Motorola has also been mass producing a capacitive accelerometer for air-bag applications [84]. This sensor has a range of ±40 g, a sensitivity of 40 mV/g, and a peak noise level of 15 mV in 400 Hz bandwidth, and utilizes a plastic dual in pin integrated circuit (IC) package to reduce cost. Other companies, including Delco and Ford, mass produce accelerometers for automotive applications. Fig. 8 shows Ford's hybrid packaged accelerometer, which consists of a sensor chip, fabricated using bulk silicon micromachining, and a CMOS sigma–delta interface chip [33]. This accelerometer is designed for automotive passive restraint systems, has a range of −50 to +30 g with 400 Hz bandwidth, provides serial digital output with sensitivity of 3 kHz/g, has a self-test feature, and is available with a low-cost plastic surface mount device (SMD) package [74]. Endevco produces a large variety of piezoelectric, piezoresistive, and capacitive accelerometers with full-scale ranges from 2 to over 4000 g for a wide range of applications, including impact and crash sensing and vibration analysis [85]. In Europe, silicon accelerometers are in volume production by Bosch, and in Japan by Denso.

CSEM in Europe has produced one of the first high-precision silicon microaccelerometers [21], [22], [24]. These devices are capacitive bulk micromachined. One of the latest versions, MS6100, is targeted for low-power applications and achieves sub-mg resolution with a TCO of 50 μg/°C and stability of 1 mg for a 2 g device with less than 0.5 mW power dissipation [86]. In the United States, some companies active in navigation and guidance, such as Litton, have also been pursuing development of μg accelerometers [25].

E. Challenges and Future Trends

Today, microaccelerometers, with low and medium sensitivities, are in large volume production with prices under $5. This is a good indication that their technology is maturing and that numerous challenges involved in their design and mass production are resolved. Although a number of high-precision accelerometers have been already developed [21]–[25], most are not evaluated completely as inertial grade yet, and they are expensive for several applications and still need improvement to overcome long-term stability and temperature-sensitivity problems. Therefore, the development of low-cost, inertial-grade accelerometers with sub-μg noise levels, good long-term stability, and low temperature sensitivity still remains a challenge. The development of low-stress, low-drift packaging technologies for inertial-grade devices without affecting device performance and stability is also being pursued. A major challenge is the interface circuit, where *low-drift* readout/control circuitry with high sensitivity, low noise level, and large dynamic range is needed. It is believed that highly stable (inertial-grade) multiaxis devices with sub-μg resolution and over 120 dB dynamic range in several hundred hertz bandwidth will be developed in the near future.

III. Micromachined Gyroscopes

A. Operating Principles and Specifications

Almost all reported micromachined gyroscopes use vibrating mechanical elements to sense rotation. They have no rotating parts that require bearings, and hence they can be easily miniaturized and batch fabricated using micromachining techniques. All vibratory gyroscopes are based on the transfer of energy between two vibration modes of a structure caused by Coriolis acceleration. Coriolis acceleration, named after the French scientist and engineer G. G. de Coriolis (1792–1843), is an apparent acceleration

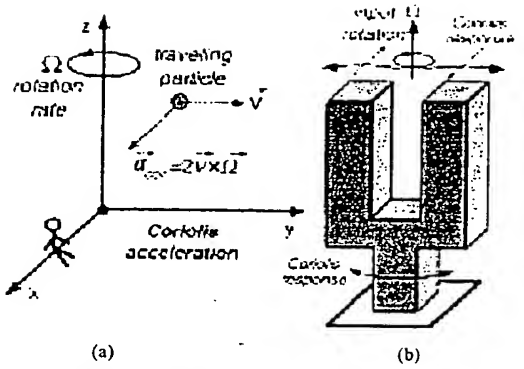

Fig. 9. (a) The Coriolis effect. (b) Tuning-fork vibratory gyroscope. The tines are differentially driven to a fixed amplitude. Coriolis force is detected either as differential bending of the tuning-fork tines or as a torsional vibration of the tuning-fork stem.

that arises in a rotating reference frame and is proportional to the rate of rotation. To understand the Coriolis effect, imagine a particle traveling in space with a velocity vector v. An observer sitting on the x-axis of the xyz coordinate system, shown in Fig. 9(a), is watching this particle. If the coordinate system along with the observer starts rotating around the z-axis with an angular velocity Ω, the observer thinks that the particle is changing its trajectory toward the x-axis with an acceleration equal to $2v \times \Omega$. Although no real force has been exerted on the particle, to an observer, attached to the rotating reference frame an apparent force has resulted that is directly proportional to the rate of rotation. This effect is the basic operating principle underlying all vibratory structure gyroscopes.

Resolution, drift, zero-rate output (ZRO), and scale factor are important factors that determine the performance of a gyroscope. In the absence of rotation, the output signal of a gyroscope is a random function that is the sum of white noise and a slowly varying function [87]. The white noise defines the resolution of the sensor and is expressed in terms of the standard deviation of equivalent rotation rate per square root of bandwidth of detection [(°/s)/$\sqrt{\text{Hz}}$ or (°/h)/$\sqrt{\text{Hz}}$]. The so-called "angle random walk" in °/$\sqrt{\text{h}}$ may be used instead. The peak-to-peak value of the slowly varying function defines the short- or long-term drift of the gyroscope and is usually expressed in °/s or °/h [87]. Scale factor is defined as the amount of change in the output signal per unit change of rotation rate and is expressed in V/(°/s). Last, an important factor for any gyroscope that is primarily defined by device imbalances is the ZRO, which represents the output of the device in the absence of a rotation rate.

In general, gyroscopes can be classified into three different categories based on their performance: inertial-grade, tactical-grade, and rate-grade devices. Table 2 summarizes the requirements for each of these categories [87], [88]. Over the past few years, much of the effort in developing micromachined silicon gyroscopes has concentrated on "rate-grade" devices, primarily because of their use in automotive applications. This application requires a full-scale range of at least 50°/s and a resolution of about 0.1°/s in a bandwidth of 50 Hz, all at a cost of $10–20 [89]. The operating temperature is in the range from −40 to 85°C. There are also several other applications that require improved performance, including inertial navigation, guidance, robotics, and some consumer electronics. Today, optical gyroscopes are the most accurate gyroscopes available in the market. Among these, ring laser gyroscopes have demonstrated inertial-grade performance, while fiber-optic gyroscopes are mainly used in tactical-grade applications. Delco's hemispherical resonator gyroscope (HRG) is a vibratory gyroscope that has achieved impressive inertial-grade performance [90]. Although highly accurate, these devices are too expensive and bulky for many low-cost applications. Achieving "tactical- and inertial-grade" performance levels has proven to be a tough challenge for micromachined gyroscopes, and new technologies and approaches are being developed. Because of their greater compatibility with batch fabrication technologies, this paper will only review silicon micromachined vibratory gyroscopes.

Table 2 Performance Requirements for Different Classes of Gyroscopes

Parameter	*Rate Grade*	*Tactical Grade*	*Inertial Grade*
Angle Random Walk, °/√h	>0.5	0.5-0.05	<0.001
Bias Drift, °/h	10-1000	0.1-10	<0.01
Scale Factor Accuracy, %	0.1-1	0.01-0.1	<0.001
Full Scale Range (°/sec)	50-1000	>500	>400
Max. Shock in 1msec, g's	10^3	10^3-10^4	10^3
Bandwidth, Hz	>70	~100	~100

B. Review of Micromachined Vibratory Gyroscopes

A number of vibratory gyroscopes have been demonstrated, including tuning forks [91]–[94], vibrating beams [95], and vibrating shells [89]. Tuning forks are a classical example of vibratory gyroscopes. The tuning fork, as illustrated in Fig. 9(b), consists of two tines that are connected to a junction bar. In operation, the tines are differentially resonated to a fixed amplitude, and when rotated, Coriolis force causes a differential sinusoidal force to develop on the individual tines, orthogonal to the main vibration. This force is detected either as differential bending of the tuning fork tines or as a torsional vibration of the tuning fork stem. The actuation mechanisms used for driving the vibrating structure into resonance are primarily electrostatic, electromagnetic, or piezoelectric. To sense the Coriolis-induced vibrations in the second mode, capacitive, piezoresistive, or piezoelectric detection mechanisms can be used. Optical detection is also feasible, but it is too expensive to implement. In general, silicon micromachining processes for fabrication of vibratory gyroscopes fall into one of four categories: 1) silicon bulk micromachining and wafer bonding; 2) polysilicon surface

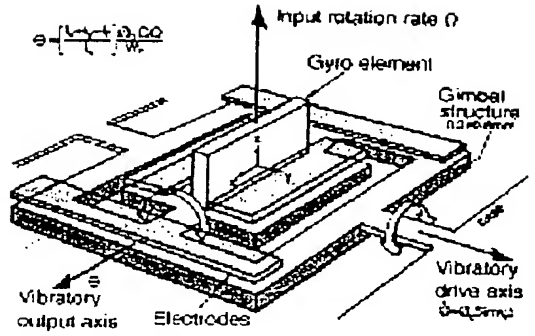

Fig. 10. Draper's first silicon micromachined double-gimbal vibratory gyroscope (1991) [100].

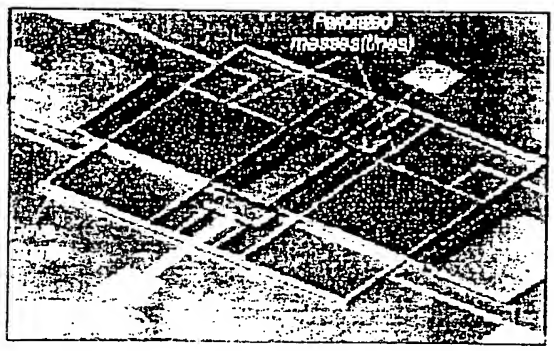

Fig. 11. SEM view of Draper's single-crystal silicon-on-glass tuning-fork gyroscope [103].

micromachining; 3) metal electroforming and LIGA; and 4) combined bulk-surface micromachining or so-called mixed processes.

Piezoelectric vibratory gyroscopes were demonstrated in the early 1980's. Examples of these devices are fused-quartz HRG by Delco [90], quartz tuning forks [96] like the Quartz Rate Sensor by Systron Donner [97], [98], and a piezoelectric vibrating disc gyro [99]. Although quartz vibratory gyroscopes can yield very high quality factors at atmospheric pressure with improved level of performance, their batch processing is not compatible with IC fabrication technology. In the late 1980's, after successful demonstration of batch-fabricated silicon accelerometers, some efforts were initiated to replace quartz with silicon in micromachined vibratory gyroscopes. The Charles Stark Draper Laboratory demonstrated one of the first batch-fabricated silicon micromachined rate gyroscopes in 1991. This bulk silicon device was a double gimbal vibratory gyroscope supported by torsional flexures, with the vibrating mechanical element made from p++ silicon [100]. As illustrated in Fig. 10, the outer gimbal was electrostatically driven at a constant amplitude using the drive electrodes, and this oscillatory motion was transferred to the inner gimbal along the stiff axis of the inner flexures. When exposed to a rotation normal to the plane of the device, Coriolis force causes the inner gimbal to oscillate about its weak axis with a frequency equal to the drive frequency. Therefore, maximum resolution is obtained when the outer gimbal is driven at the resonant frequency of the inner gimbal, causing the sensitivity to be amplified by the mechanical quality factor of the sense resonance mode of the structure. A rotation rate resolution of 4°/s in a 1 Hz bandwidth was realized using this structure.

Later in 1993, Draper reported an improved 1 mm^2 silicon-on-glass tuning fork gyroscope [91] fabricated through the dissolved wafer process [101]. This gyroscope was electrostatically vibrated in its plane using a set of interdigitated comb drives [102] to achieve a large amplitude of motion (10 μm). Any rotation in the plane of the substrate perpendicular to the drive mode will then excite the out-of-plane rocking mode of the structure, which is capacitively monitored. Fig. 11 shows an SEM view of the device with a perforated mass to minimize damping. The in-plane motion of the structure is lightly damped by air, while out-of-plane motion is strongly damped due to squeeze film effects. Therefore, for out-of-plane modes, Q rises rapidly as pressure is reduced, in contrast to the in-plane Q, which shows a small increase as the pressure drops. At pressures of 100 mTorr, a Q of 40 000 was observed for the drive mode and 5000 for the sense mode. The silicon-on-glass technology used in this device has the advantage of low stray capacitance. The noise equivalent rate observed by this structure was 470°/h in a 60 Hz bandwidth, equivalent to 0.02°/s in a 1 Hz bandwidth or angle random walk of $0.72°/\sqrt{h}$ [103]. The scale-factor accuracy was better than 0.1%, and bias stability was 55°/h overnight. The projected performance was 10–100°/h for bias stability and resolution in a 60 Hz bandwidth.

If the sense and drive resonant modes of a tuning fork have equal frequencies, the output signal will be amplified by the quality factor Q of the sense mode, resulting in much higher sensitivity. However, this involves extreme control of device dimensions and may lead to temperature drift problems if these natural frequencies do not track with temperature. Because of these difficulties, most tuning-fork designs are not based on matched vibration mode frequencies.

Other tuning-fork designs have used electromagnetic excitation to obtain a large amplitude of motion [92], [93], [104]. Bosch's silicon yaw rate sensor [93] achieves vibration amplitudes as large as 50 μm using a permanent magnet mounted inside a metal package. This device was fabricated through a combination of bulk- and surface-micromachining processes, and it consists of two bulk-micromachined oscillating masses, each of which supports two surface-micromachined accelerometers for detection of Coriolis force. The sensor chip is anodically bonded to a supporting glass wafer and is covered by another silicon cap wafer. Operating at atmospheric pressure, the device has shown a resolution of 0.3°/s in a 100 Hz bandwidth, thanks to its large amplitude of vibration. Although such a large amplitude of oscillation (50 μm) can increase the

output signal level, it increases the total power consumption and may cause fatigue problems over long-term operation. Cross talk between the sense and drive modes was minimized through mechanical decoupling of these modes by separating the oscillator and sense proof masses, resulting in a stable ZRO.

Piezoresistive detection has also been used in some gyroscope designs. Daimler Benz has demonstrated a tuning-fork angular rate sensor for automotive applications that piezoresistively measures the rotation-induced shear stress in the stem of the tuning-fork device [94]. In this device, a piezoelectric actuation mechanism was used by depositing a piezoelectric aluminum nitride (AlN) thin-film layer on one of the tines. The use of piezoelectric thin films such as AlN and ZnO on silicon degrades Q and causes large temperature variation of offset and sensitivity [105]. This device was fabricated through a combination of bulk micromachining and bonding of SOI wafers. Researchers at the University of Neuchatel, Switzerland, have demonstrated a tuning-fork design based on two isolated vibrating proof masses, each supported by a four-beam bridge-type suspension [104]. These proof masses are electromagnetically vibrated in plane and antiphase, and the rotation-induced out-of-plane motion is then detected by means of four piezoresistors connected in a Wheatsone bridge configuration, showing a sensitivity of 4 nV/°/s with excellent linearity up to 750°/s. This device was fabricated through silicon bulk micromachining and was wafer-level vacuum packaged by anodic bonding of the silicon wafer to encapsulating glass wafers. In general, package-induced stress on the sensor structure can be lowered by low-temperature anodic bonding of glass wafers with silicon [106]. Although piezoresistive devices are easier to fabricate and require a simpler electronic interface due to their lower output impedance compared to capacitive devices, they have large temperature sensitivity and poor resolution.

Also reported in the literature are capacitive bulk-micromachined silicon-on-glass vibrating beams [107], vibrating membranes [108], and double-gimbaled structures [109]. Since the Young's modulus of single-crystal silicon changes with crystallographic orientation, symmetric vibrating structures made of single-crystal silicon may show excessive mechanical coupling between drive and sense modes (due to this anisotropy), resulting in a large ZRO with unacceptable drift characteristics [107].

Surface-micromachined vibratory gyroscopes have also been demonstrated. Some have been integrated with the readout electronic circuitry on a single silicon chip, reducing parasitic capacitances and hence increasing the signal-to-noise ratio. In addition, the vibrating structure is made of polysilicon, which has a high quality factor and an orientation-independent Young's modulus. Single- and dual-axis polysilicon surface-micromachined gyroscopes have been realized by researchers at Berkeley [110], [111] and Samsung [112]–[114]. Berkeley's z-axis vibratory rate gyroscope [110] resembles a vibrating beam design and consists of an oscillating mass that is

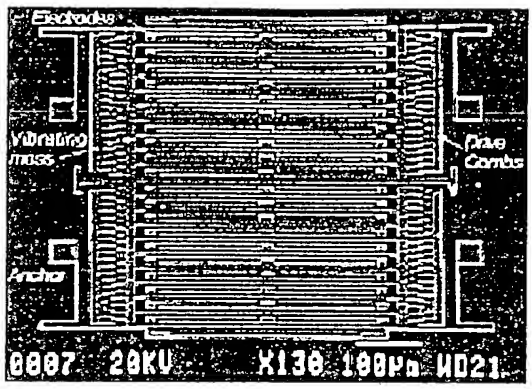

Fig. 12. SEM view of a comb-driven polysilicon surface micromachined z-axis vibratory gyroscope [113].

electrostatically driven into resonance using comb drives. Any deflections that result from Coriolis acceleration are detected differentially in the sense mode using interdigitated comb fingers. This device, 1 mm across, was integrated with a transresistance amplifier on a single die using the Analog Devices BiMEMS process. The remaining control and signal-processing electronics were implemented off chip. Quadrature error nulling and sense-mode resonant frequency tuning can be accomplished in this design by applying a control dc bias voltage to the position sense fingers. The dc bias voltage generates an electrostatic negative stiffness, which reduces the resonant frequency of the sense mode. By slightly changing this dc bias voltage on the differential comb fingers ($\pm\Delta$ V), a lateral electrostatic field arises that can be used to align the drive mode oscillations and reduce the quadrature error. This device demonstrated a resolution of $1°/s/\sqrt{Hz}$ with performance projected to improve to $0.1°/s/\sqrt{Hz}$ in a second-generation device.

Samsung has also reported a very similar surface-micromachined z-axis device, shown in Fig. 12, with a 7-μm-thick polysilicon resonating mass supported by four fishhook-shaped springs [113]. This device, though not integrated with electronics, has demonstrated a resolution of 0.1°/s at 2 Hz, an operating bandwidth of 100 Hz, and a linearity of 1% full scale in a range of 90°/s. Hybrid attachment of the sensor chip to a CMOS application-specific integrated circuit (ASIC) chip used for readout and closed-loop operation of the gyro was done in a vacuum-packaged ceramic case.

Murata has presented a surface-micromachined polysilicon gyroscope that is sensitive to lateral (x- or y-axis) angular rate [115]. The sense electrode was made underneath the perforated polysilicon resonator by diffusing phosphorous into the silicon substrate (junction isolation). This device showed an open-loop noise-equivalent rate of $2°/s/\sqrt{Hz}$. The junction-isolation scheme used in this device, although simple, has the disadvantage of relatively large parasitic capacitance and large amount of shot noise associated with the existing pn junction, which in turn

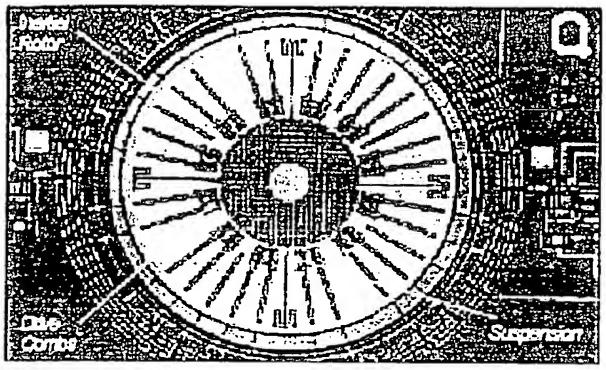

Fig. 13. Closeup die shot of Berkeley's dual-axis rate gyroscope, integrated with sense and drive electronics using Analog Devices, Inc., surface-micromachining process [116].

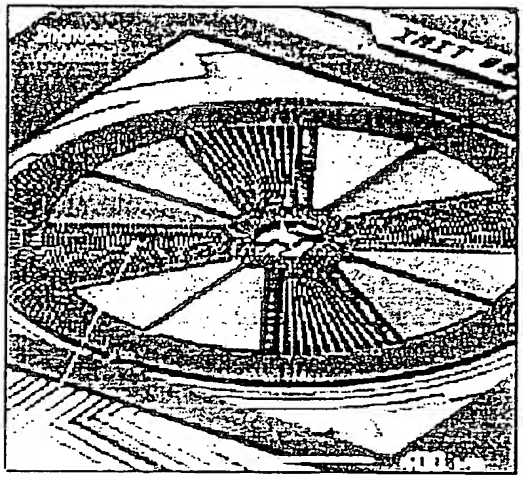

Fig. 14. SEM of HSG-IMIT's surface-micromachined x-axis vibratory gyroscope (MARS-RR) fabricated through Bosch's process with a 10-μm-thick structural polysilicon layer [120].

degrade the resolution. Later in 1997, Samsung reported a similar device that used a 3000-Å-thick polysilicon sense electrode underneath a 7.5-μm-thick low-pressure chemical vapor deposition (LPCVD) polysilicon resonating mass [112]. Since the detection mode is highly damped by squeeze film damping, these devices have to operate under vacuum. Samsung's device, vacuum packaged in an Al_2O_3 case, showed an improved open-loop noise-equivalent rate of 0.1°/s/$\sqrt{\text{Hz}}$ with a good linearity up to 100°/s.

Berkeley has reported a surface-micromachined dual-axis gyroscope based on rotational resonance of a 2-μm-thick polysilicon rotor disk, as shown in [116] (Fig. 13). Since the disk is symmetric in two orthogonal axes, the sensor can sense rotation equally about these two axes. This device, integrated with electronics, yielded a random walk as low as 10°/$\sqrt{\text{h}}$ with cross-axis sensitivity ranging 3–16%. Resolution can be further improved to 2°/$\sqrt{\text{h}}$ by frequency matching at the cost of excessive cross-axis sensitivity. Also reported in the literature is a cross-shaped nickel-on-glass two-axis micromachined gyroscope [117], which has shown a rate sensitivity of 0.1 mV/°/s.

The JPL, in collaboration with the University of California, Los Angeles, has demonstrated a bulk-micromachined, precision silicon MEMS vibratory gyroscope for space applications [118], [119]. This clover-leaf-shaped gyroscope consists of three major components: a silicon clover-leaf vibrating structure; a silicon baseplate, which is bonded to the clover-leaf structure; and a metal post, which is epoxied inside a hole on the silicon resonator. A hermetically sealed package, 1 × 1 × 0.7 in, houses the microgyroscope and most of its control electronics. This packaged gyroscope has a 7 Hz split between its drive and sense mode (f_{res} = 1.44 kHz), a scale factor of 24 mV/°/s, a bias stability of 70°/h, and an angle random walk of 6.3°/$\sqrt{\text{h}}$.

Recently, researchers at HSG-IMIT, Germany, have demonstrated and reported a surface-micromachined precision x-axis vibratory gyroscope (MARS-RR) with a very small ZRO achieved by mechanical decoupling of the drive and sense vibration modes [120]. This device (6 mm^2), shown in Fig. 14, was fabricated through the standard Bosch foundry process featuring a 10-μm-thick structural polysilicon layer in addition to the buried polysilicon layer, which defines the sense electrodes. The reported performance of this device is quite impressive: a random angle walk of 0.27°/$\sqrt{\text{h}}$, a bias stability of 65°/h, and a scale-factor nonlinearity of <0.2%.

Researchers at General Motors and the University of Michigan have developed a vibrating ring gyroscope [89], schematically shown in Fig. 15. This device consists of a ring, semicircular support springs, and drive, sense, and balance electrodes, which are located around the structure. Symmetry considerations require at least eight springs to result in a balanced device with two identical flexural modes that have equal natural frequencies [121]. The ring is electrostatically vibrated into an in-plane elliptically shaped primary flexural mode with a fixed amplitude. When it is subjected to rotation around its normal axis, Coriolis force causes energy to be transferred from the primary mode to the secondary flexural mode, which is located 45° apart from the primary mode, causing amplitude to build up proportionally in the latter mode; this buildup is capacitively monitored. The vibrating ring structure has some important features compared to other types of vibratory gyroscopes. First, the inherent symmetry of the structure makes it less sensitive to spurious vibrations. Only when the ring has mass or stiffness asymmetries can environmental vibrations induce a spurious response. Second, since two identical flexural modes of the structure "with nominally equal resonant frequencies" are used to sense rotation, the sensitivity of the sensor is amplified by the quality factor of the structure, resulting in higher sensitivity. Third, the vibrating ring is less temperature sensitive since the vibration modes are affected equally by temperature. Last, electronic balancing of the structure is possible. Any frequency mismatch due to mass or stiffness asymmetries that occurs during the fabrica-

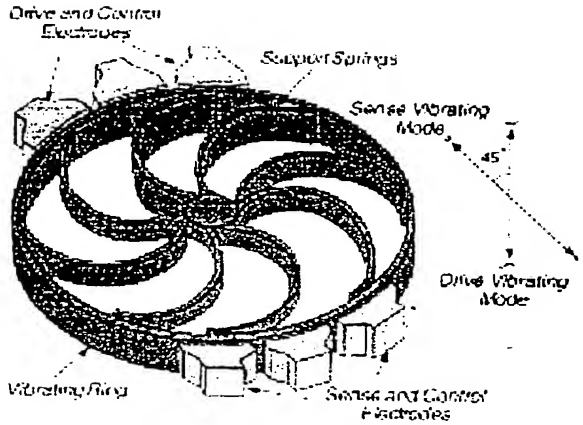

Fig. 15. Structure of a vibrating ring gyroscope.

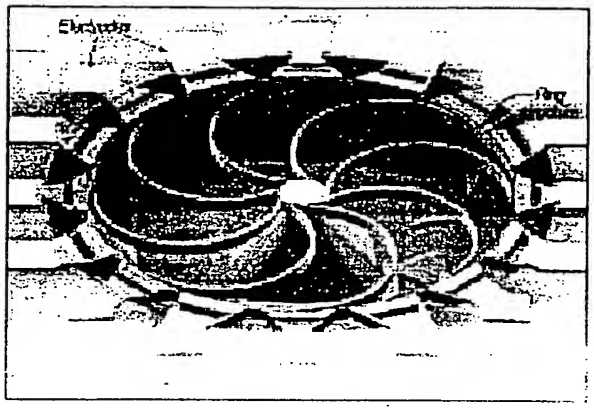

Fig. 16. SEM view of a PRG [123]. The polysilicon ring is 1 mm in diameter, 3 μm wide, and 35 μm tall.

tion process can be electronically compensated by use of the balancing electrodes that are located around the structure.

The first micromachined version of the vibrating ring gyroscope was fabricated by electroforming nickel into a thick polyimide (or photoresist) mold on a silicon substrate in a post circuit process [89], [121], [122]. The gyroscope demonstrated a resolution of $\sim$0.5°/s in a 25 Hz bandwidth limited by the readout electronic noise. The sensor was integrated with a low-input capacitance source-follower buffer and the amplifier on a silicon chip. The zero bias drift was <10°/s over the temperature range −40 to 85°C, and the sensitivity of the device varied by less than 3% over the same temperature range. Scale-factor nonlinearity in a ±100°/s rate range was <0.2% [122].

To improve performance further, a new polysilicon ring gyroscope (PRG) [123] was recently fabricated through a single-wafer, all-silicon, high-aspect-ratio p^{++}/polysilicon trench-refill technology [124] at the University of Michigan. In this new process, the vibrating ring and support springs are created by refilling deep dry-etched trenches with polysilicon deposited over a sacrificial LPCVD oxide layer. Each sense electrode is made from a p^{++} silicon island (12 μm deep) hanging over an ethylenediamine-pyrocatechol (EDP)-etched pit. Fig. 16 shows a SEM picture of a 1.7 × 1.7 mm^2 PRG. This device provides several important features required for high-performance gyroscopes, including small ring-to-electrode gap spacing (<1 μm) for increasing the sense capacitance; large structural height for increasing the radius and sense capacitance and reducing the resonant frequency; and a better structural material (polysilicon) for increasing Q with an orientation-independent Young's modulus. By taking advantage of these features, a tactical-grade ring microgyroscope with projected random walk as small as 0.05°/$\sqrt{h}$ can be potentially realized, providing orders of magnitude improvement in performance.

British Aerospace Systems and Equipment, in collaboration with Sumitomo Precision Products, has also developed a micromachined single-crystalline silicon ring gyroscope with a reported root-mean-square noise floor of 0.15°/s in a 30 Hz bandwidth and an in-run drift of approximately 0.05°/s [125]. This device was fabricated through deep dry etching of a 100-μm-thick silicon wafer, which was then anodically bonded to a glass support wafer.

Levitated micromachined spinning-disc gyroscopes have also been investigated [126], [127]. The concept was based on a rotor disc, levitated using electromagnetic or electrostatic means and spun at a very high rate by means of a motor to produce angular momentum. With additional electrostatic fields, the rotor can be held in equilibrium even if the sensor is tilted or inverted. It is predicted that spinning microgyroscopes can yield a lower drift than a vibrating structure gyroscope [127]. The performance of these devices is yet to be demonstrated.

C. Design Issues and Considerations

Vibratory gyroscopes can be operated open or closed loop to measure rate of rotation (angular velocity). In the open-loop mode, the response to a change in rotation rate is not instantaneous, as time is required for the amplitude of the sense mode to reach its steady-state value. With matched sense and drive resonant modes, the time constant associated with this amplitude buildup is approximately equal to $2Q/\omega$ [121]. This response time limits the bandwidth of the sensor to a few hertz. To obtain larger open-loop bandwidth, gyroscopes are sometimes operated with a slight mismatch in the sense and drive mode resonant frequencies; however, as theoretically shown in [128], this is done at the cost of reduced sensitivity. In the closed-loop mode of operation, the sense mode amplitude is continuously monitored and driven to zero, and hence the bandwidth and dynamic range of the sensor can be increased beyond the open-loop values even with matched resonant modes. The bandwidth is then limited by the readout and control electronics and can be increased to values approaching the resonant frequency of the structure.

With matched sense and drive resonant modes, assuming that the readout electronic noise V_n has a white spectrum

around the resonant frequency of the structure and that the detection circuit has a bandwidth of BW, the minimum detectable electronic signal for a capacitive device can be expressed by

$$\Omega_{z(\min)} \propto \frac{\omega}{Q} \cdot \frac{(C_{\text{rest}} + C_{\text{paras.}})}{\delta c_{\text{rest}}} \cdot V_n \sqrt{\text{BW}}. \quad (4)$$

This equation shows that reducing the noise of the readout circuit, increasing the Coriolis-induced capacitance change of the device, lowering the resonant frequency, increasing the mechanical quality factor, and minimizing the parasitic capacitances are determining factors in improving the resolution. If the closed-loop bandwidth is not extended beyond the open-loop bandwidth ($\sim\omega/2Q$), then the resolution in the closed-loop mode is also expressed by the theoretical maximum open-loop value (4) [121]. Although the resonant frequency of the structure should be lowered for improved sensitivity, it must be kept above environmental noise (>2 kHz). Stronger Coriolis forces will be obtained by increasing the amplitude of vibration in the drive mode (q_{drive}), thus improving the resolution.

It should be noted that the fundamental limiting noise component of the mechanical structure is due to the Brownian motion of the sense vibration mode, and its total noise equivalent acceleration is given by (3). This acceleration noise corresponds to an input rotation rate noise whose spectral density is determined using the transfer function (from input rotation rate to the sense mode acceleration) of each particular device. At high quality factors (operation in vacuum), resolution is usually not limited by Brownian motion of the structure; it is limited by the readout electronic noise.

An important performance parameter for a vibratory gyroscope is its zero rate output (or zero bias). Geometrical imperfections in the vibrating mechanical structure and/or the sense and drive electrodes as well as electrical coupling between these electrodes can cause an output signal in the absence of rotation. For instance, in tuning-fork designs, if due to fabrication flaws the tines' centers of mass are not precisely aligned in the plane of vibration, their inertial forces produce a vibrating torque about the stem just as the Coriolis torque does. This error, often called the quadrature error, can be distinguished from the rate signal simply because it is in phase quadrature with the Coriolis-induced signal. If too large, it may cause errors in sensing the rotation rate and can even saturate the amplifier [110]. In the case of shell gyroscope designs, asymmetric damping of the structure, which manifests itself as different sense and drive mode quality factors, can also cause a finite output when there is no rotation [88]. By electrically and mechanically decoupling the sense and drive modes, and by minimizing the fabrication process errors, ZRO can be significantly reduced [93], [120]. A large quality factor and lower natural frequency can further reduce the ZRO, and its drift simply due to the fact that these two factors increase the open-loop sensitivity of the sensor. Therefore, high-quality materials with low internal damping will improve the accuracy of the sensor. Any remaining zero bias error should then be further reduced electronically. For instance, the nickel ring gyroscope can be electronically trimmed to reduce the zero bias from 60°/s to less than 0.5°/s.

A high-performance gyroscope should have an accurate scale factor over a wide dynamic range as large as 140 dB. The scale factor should have a small temperature sensitivity. Special attention should be paid to the structural material. Metal structures used on silicon substrates or piezoelectric layers cemented on silicon structures can cause large variation of scale factor with temperature. All-silicon devices are suitable for high-performance applications. Variation of resonant frequency over temperature (due to temperature dependence of Young's modulus) can also affect the scale factor of the sensor, and therefore, some temperature compensation of the scale factor is required [121].

To obtain a high mechanical quality factor, both external and internal energy losses should be minimized. Balanced, symmetrical, isolated structures that do not radiate acoustic energy out of their anchors are therefore required. In balanced symmetrical structures, the dependence of the output signal on rigid body motion of the structure caused by linear acceleration can be electronically rejected. An example of a balanced system is a tuning-fork design, made from two symmetrical tines oscillating antiphase, which has no net motion at the junction and therefore can be mounted inertially stable at this junction. Energy losses due to squeeze film damping by air molecules will be significantly reduced if the resonant device is operated in vacuum. This calls for hermetically sealed, low-stress, robust vacuum-packaging techniques that are capable of holding vacuum levels (10^{-2}–10^{-3} Torr) for extended periods of time. Silicon or glass wafers [93], [104] bonded to the sensor substrate can provide hermetically sealed, chip-level encapsulation [129]. Internal energy loss is reduced if the structure is fabricated from low-loss materials such as single- and polycrystalline silicon. Another concern about a vibrating mechanical element is the long-term drift and fatigue problem. Small vibration amplitude can help reduce these problems.

Last, readout, signal-processing, and control electronics are needed for open- and closed-loop operation of a vibratory gyroscope. Part of the electronics drives the first mode of the structure into resonance and keeps the amplitude of vibration constant. Extremely small Coriolis-induced motions of the structure are then detected by the readout electronics. Low-noise readout techniques require a careful biasing scheme using diodes [89], resistors [130], and subthreshold MOS devices [110]. Monolithic integration of the sensor and the readout electronics reduces the interconnect parasitics and improves the resolution of the sensor. Parasitic capacitances can be further reduced by special bootstrapping techniques [121], [130]. Delco Electronics has demonstrated a CMOS ASIC chip for closed-loop operation of an electroformed ring gyroscope [131]. It consists of four feedback loops and provides the necessary electronics to compensate for the sensor

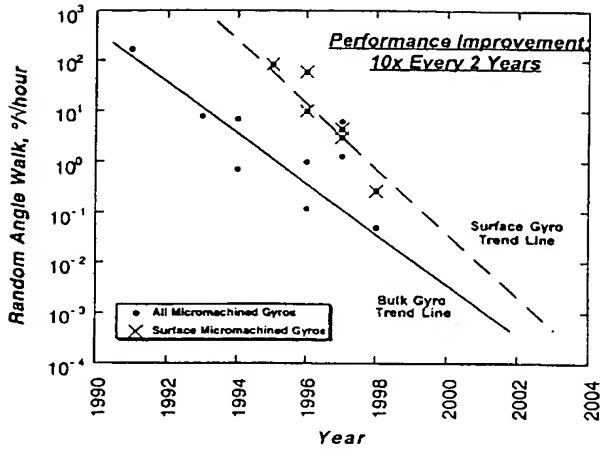

Fig. 17. Performance of micromachined gyroscopes has improved by a factor of ten every two years since 1991.

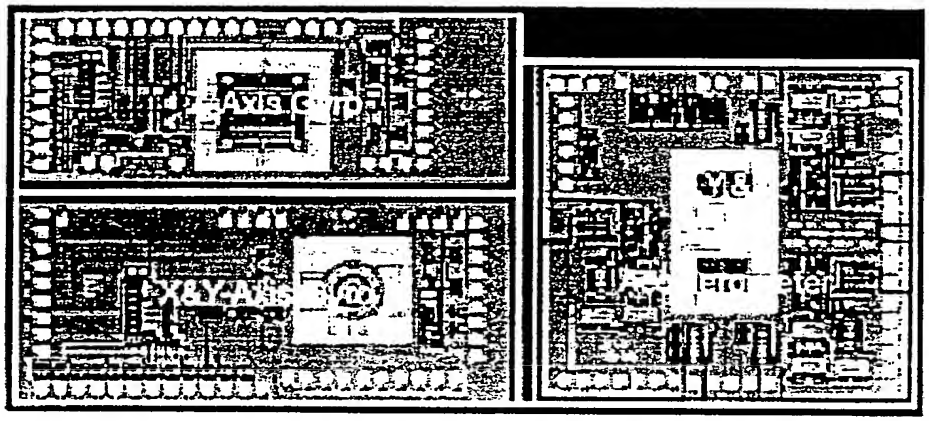

Fig. 18. A six-degree-of-freedom, fingernail-sized IMU with integrated signal-processing and control circuitry, designed at the University of California, Berkeley, and fabricated by Sandia National Laboratories. (Courtesy of T. Juneau.)

nonuniformities and its offset and sensitivity variations with temperature (−40 to +85°C). High-performance gyroscopes will continue to need precision, low-noise, parasitic-insensitive interface circuits capable of resolving attofarad changes in capacitance with as small an input capacitance as possible.

D. Commercialization and Future Trends

Mainly driven by the automotive industry, micromachined silicon gyroscopes have been the subject of extensive research and development over the past few years. The performance of micromachined gyroscopes has drastically improved over a rather short period, as illustrated in Fig. 17, which is based on a sample of devices reported in the literature. Since 1991, performance, indicated by the random angle walk, has improved by a factor of 10× every two years for both bulk- and surface-micromachined devices. The plot also shows that surface-micromachined devices have been closing the gap with their bulk counterparts. Although this general trend is not expected to continue indefinitely, it is anticipated that for at least the next 5–10 years, we will see a continuing improvement in the performance of both bulk- and surface-micromachined gyroscopes.

Much effort is also under way for large-volume production of micromachined gyroscopes. Production cost, performance, and reliability are the key factors in commercializing micromachined gyroscopes. Precision micromachining, robust vacuum packaging, and high-performance interface circuit and electronic tuning techniques are required to reduce the production cost to a level that is acceptable for the large-volume automotive market [132]. Since 1993, Draper and Rockwell International have been collaborating to commercialize Draper's silicon tuning-fork gyroscope targeted for automotive applications [133]. Other companies like General Motors, Analog Devices,

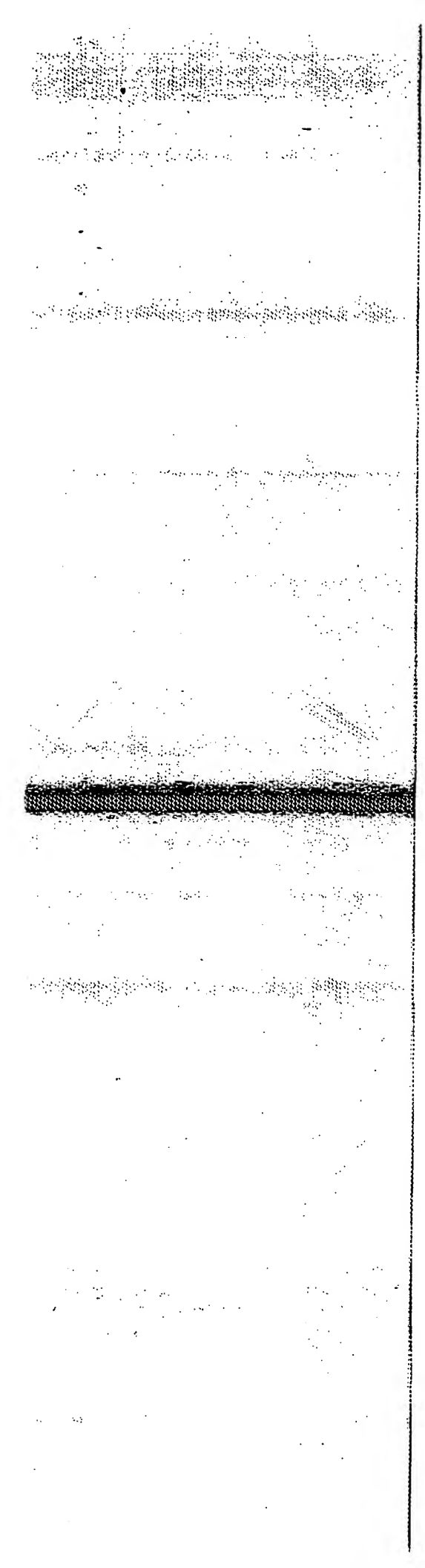

much effort will be expended to
omachining further, develop low-
face circuitry, and provide reliable
development of even higher per-
id lower power inertial sensors for
yet unknown applications.

dge all those who contributed their
photographs shown in this paper,
Yeh, Dr. A. Selvakumar, and Dr.

achined gyroscopes," *Sensors Actuators* 1994.
anical-thermal noise in micromachined ensors," *IEEE Trans. Electron Devices,* May 1993.
rication, and optimization of microme- D. thesis, University of California at

A. Angell, "A batch-fabricated silicon *ans. Electron Devices,* vol. ED-26, pp.

i, "Design optimization for cantilever- *ensors Actuators,* vol. 6, pp. 81–92,

nd E. Obermeier, "A silicon based mi- eter with cross acceleration sensitivity *Dig. 4th Int. Conf. Solid-State Sensors ers '87),* Tokyo, Japan, June 1987, pp.

Colbeck, G. Muck, W. Kupke, and M. icon accelerometer with highly sym- *ctuators,* vol. A21/A23, pp. 312–315,

3. Puers, and W. Sansen, "A highly icro-accelerometer with single degree- *Micromech. Microeng.,* vol. 2, pp.

oshenko, *Mechanics of Materials,* 3rd nd Hall, 1991.
ical Design Handbook. New York:

rdson, and S. Yamanami, "A study of g," *J. Basic Eng., Trans. ASME,* pp.

damping in solid-state accelerome- *tate Sensors and Actuators Workshop,* une 1990, pp. 44–47.
adenski, and F. Maseeh, "A virtual oftware system for MEMS," in *Proc. nical Systems Workshop (MEMS'96),* , pp. 122–126.
adi, R. Mayer, J. Poydock, and K. licon accelerometer with integral air otection," in *Tech. Dig. Solid-State kshop,* Hilton Head Island, SC, June

el, and K. Petersen, "Silicon ac- mal self-test mechanism," in *Tech. d Actuators Workshop,* Hilton Head 122–125.
De Bruin, "Accelerometer system " *Sensors Actuators,* vol. 20, pp.

e, U. Schnakenberg, and B. Wagner, h on-chip electronics fabricated by ss," *Sensors Actuators,* vol. A-31,

[18] H. Seidel, U. Fritsch, R. Gottinger, and J. Schalk, "A piezoresistive silicon accelerometer with monolithically integrated CMOS-circuitry," in *Tech. Dig. 8th Int. Conf. Solid-State Sensors and Actuators (Transducers'95)*, Stockholm, Sweden, June 1995, pp. 597–600.

[19] S. J. Sherman, W. K. Tsang, T. A. Core, R. S. Payne, D. E. Quinn, K. H. Chau, J. A. Farash, and S. K. Baum, "A low-cost monolithic accelerometer: Product/technology update," in *Tech. Dig. IEEE Electron Devices Meeting (IEDM'92)*, Dec. 1992, pp. 160–161.

[20] L. Ristic, R. Gutteridge, J. Kung, D. Koury, B. Dunn, and H. Zunino, "A capacitive type accelerometer with self-test feature based on a double-pinned polysilicon structure," in *Tech. Dig. 7th Int. Conf. Solid-State Sensors and Actuators (Transducers'93)*, Yokohama, Japan, June 1993, pp. 810–812.

[21] F. Rudolf, A. Jornod, and P. Bencze, "Silicon microaccelerometers," in *Tech. Dig. 4th Int. Conf. Solid-State Sensors and Actuators (Transducers'87)*, Tokyo, Japan, June 1987, pp. 376–379.

[22] F. Rudolf, A. Jornod, J. Berqovist, and H. Leuthold, "Precision accelerometers with μg resolution," *Sensors Actuators*, vol. A21/A23, pp. 297–302, 1990.

[23] W. Henrion, L. DiSanza, M. Ip, S. Terry, and H. Jerman, "Wide-dynamic range direct digital accelerometer," in *Tech. Dig. Solid-State Sensors and Actuators Workshop*, Hilton Head Island, SC, June 1990, pp. 153–156.

[24] Y. de Coulon, T. Smith, J. Hermann, M. Chevroulet, and F. Rudolf, "Design and test of a precision servoaccelerometer with digital output," in *Tech. Dig. 7th Int. Conf. Solid-State Sensors & Actuators (Transducers'93)*, Yokohama, Japan, June 1993, pp. 832–835.

[25] K. Warren, "Navigation grade silicon accelerometer with sacrifically etched SIMOX and BESOI structure," in *Tech. Dig. Solid-State Sensors and Actuators Workshop*, Hilton Head Island, SC, June 1994, pp. 69–72.

[26] N. Yazdi and K. Najafi, "An all-silicon single-wafer fabrication technology for precision microaccelerometers," in *Tech. Dig. 9th Int. Conf. Solid-State Sensors and Actuators (Transducers'97)*. Chicago, IL, June 1977, pp. 1181–1184.

[27] K. J. Ma, N. Yazdi, and K. Najafi, "A bulk-silicon capacitive microaccelerometer with built-in overrange and force feedback electrodes," in *Tech. Dig. Solid-State Sensors and Actuators Workshop*, Hilton Head Island, SC, June 1994, pp. 160–163.

[28] C. Buhrbaum, J. Mohr, P. Bley, and W. Ehrfeld, "Fabrication of capacitive acceleration sensors by the LIGA technique," *Sensors Actuators A*, vol. 25/27, pp. 559–563, 1990.

[29] B. Boser and R. T. Howe, "Surface micromachined accelerometers," *IEEE J. Solid-State Circuits*, vol. 31, pp. 366–375, Mar. 1996.

[30] K. Chau, S. R. Lewis, Y. Zhao, R. T. Howe, S. F. Bart, and R. G. Marcheselli, "An integrated force-balanced capacitive accelerometer for low-g applications," in *Tech. Dig. 8th Int. Conf. on Solid-State Sensors and Actuators (Transducers'95)*, Stockholm, Sweden, June 1995, pp. 593–596.

[31] B. P. van Drieenhuizen, N. Maluf, I. E. Opris, and G. Kovacs, "Force-balanced accelerometer with mG resolution fabricated using silicon fusion bonding and deep reactive ion etching," in *Tech. Dig. 9th Int. Conf. Solid-State Sensors and Actuators (Transducers'97)*, Chicago, IL, June 1997, pp. 1229–1230.

[32] J. C. Cole, "A new sense element technology for accelerometer subsystems," in *Tech. Dig. 6th Int. Conf. Solid-State Sensors and Actuators (Transducers'91)*, San Francisco, CA, June 1991, pp. 93–96.

[33] L. Spangler and C. J. Kemp, "ISAAC–Integrated silicon automotive accelerometer," in *Tech. Dig. 8th Int. Conf. Solid-State Sensors and Actuators (Transducers'95)*, Stockholm, Sweden, June 1995, pp. 585–588.

[34] A. Selvakumar, F. Ayazi, and K. Najafi, "A high sensitivity z-axis torsional silicon accelerometer," in *Tech. Dig. IEEE Int. Electron Device Meeting*, San Francisco, CA, Dec. 1996, pp. 765–768.

[35] T. Smith, O. Nys, M. Chevroulet, Y. DeCoulon, and M. Degrauwe, "A 15b electromechanical sigma–delta converter for acceleration measurements," in *Tech. Dig. IEEE Int. Solid-State Circuits Conf. (ISSCC'94)*, San Francisco, CA, Feb. 1994, pp. 160–161.

[36] W. Yun, R. T. Howe, and P. R. Gray, "Surface micromachined digitally force-balanced accelerometer with integrated CMOS detection circuitry," in *Tech. Dig. Solid-State Sensor and Actuator Workshop*, Hilton Head Island, SC, June 1992, pp. 126–131.

[37] C. Lu, M. Lemkin, and B. Boser, "A monolithic surface micromachined accelerometer with digital output," *IEEE J. Solid-State Circuits*, vol. 30, pp. 1367–1373, Dec. 1995.

[38] M. Lemkin, B. Boser, and J. Smith, "A 3-axis surface micromachined $\Sigma\Delta$ accelerometer," in *Tech. Digest Int. Solid State Circuits Conf. (ISSCC'97)*, San Francisco, CA, Feb. 1997, pp. 202–203.

[39] "ADXL05-monolithic accelerometer with signal conditioning," Analog Devices, Norwood, MA, data sheet, 1995.

[40] M. A. Lemkin, M. A. Ortiz, N. Wongkomet, B. E. Boser, and J. H. Smith, "A 3-axis force balanced accelerometer using a single proof-mass," in *Tech. Dig. 9th Int. Conf. Solid-State Sensors and Actuators (Transducers'97)*, Chicago, IL, June 1997, pp. 1185–1188.

[41] T. W. Kenny, S. B. Waltman, J. K. Reynolds, and W. J. Kaiser, "A micromachined silicon electron tunneling sensor," in *Proc! IEEE Micro Electro Mechanical Systems Workshop (MEMS'90)*, Napa Valley, CA, 1990, pp. 192–196.

[42] H. K. Rocksatd, T. W. Kenny, J. K. Reynolds, W. J. Kaiser, and T. B. Gabrielson, "A miniature high-sensitivity broad-band accelerometer based on electron tunneling transducers," *Sensors Actuators A*, vol. 43, pp. 107–114, 1994.

[43] H. K. Rocksatd, J. K. Reynolds, T. K. Tang, T. W. Kenny, W. J. Kaiser, and T. B. Gabrielson, "A miniature, high-sensitivity, electron-tunneling accelerometer," in *Tech. Dig. 8th Int. Conf. Solid-State Sensors and Actuators (Transducers'95)*, Stockholm, Sweden, June 1995, pp. 675–678.

[44] C. Yeh and K. Najafi, "A low-voltage bulk-silicon tunneling-based microaccelerometer," in *Tech. Dig. IEEE Int. Electron Devices Meeting (IEDM)*, Washington, DC, Dec. 1995, pp. 593–596.

[45] R. L. Kubena, G. M. Atkinson, W. P. Robinson, and F. P. Stratton, "A new miniaturized surface micromachined tunneling accelerometer," *IEEE Electron Device Lett.*, vol. 17, pp. 306–308, June 1996.

[46] C. Yeh and K. Najafi, "A low-voltage tunneling-based silicon microaccelerometer," *IEEE Trans. Electron Devices*, vol. 44, no. 11, pp. 1875–1882, Nov. 1997.

[47] ——, "Micromachined tunneling accelerometer with a low-voltage CMOS interface circuit," in *Tech. Dig. 9th Int. Conf. Solid-State Sensors & Actuators (Transducers'97)*, Chicago, IL, June 1997, pp. 1213–1216.

[48] G. Binning and H. Rohrer, "Scanning tunneling microscopy," *IBM J. Res. Develop.*, vol. 30, pp. 355–369, 1986.

[49] J. Grade, A. Barzilai, J. K. Reynolds, C. H. Liu, A. Partridge, L. M. Miller, J. A. Podosek, and T. Kenny, "Low frequency drift in tunnel sensors," in *Tech. Dig. 9th Int. Conf. Solid-State Sensors and Actuators (Transducers'97)*, Chicago, IL, June 1997, pp. 871–874.

[50] S. Danel, F. Michel, and G. Delapierre, "Micromachining of quartz and its application to an acceleration sensor," *Sensors Actuators*, vol. A21/A23, pp. 971–977, 1990.

[51] K. Kourepenis, A. Petrovich, and M. Weinberg, "Low cost quartz resonant accelerometer for aircraft inertial navigation" in *Tech. Dig. 6th Int. Conf. Solid-State Sensors and Actuators (Transducers'91)*, San Francisco, CA, June 1991, pp. 551–553.

[52] D. W. Satchell and J. C. Greenwood, "A thermally-excited silicon accelerometer," *Sensors Actuators*, vol. 17, pp. 241–245, 1989.

[53] S. C. Chang, M. W. Putty, D. B. Hicks, and C. H. Li, "Resonant-bridge two-axis microaccelerometer," *Sensors Actuators*, vol. A21/A23, pp. 342–345, 1990.

[54] T. V. Roszhart, H. Jerman, J. Drake, and C. de Cotiis, "An inertial-grade micromachined vibrating beam accelerometer," in *Tech. Dig. 8th Int. Conf. Solid-State Sensors and Actuators (Transducers'95)*, Stockholm, Sweden, June 1995, pp. 656–658.

[55] D. W. Burns, R. D. Horning, W. R. Herb, J. D. Zook, and H. Guckel, "Resonant microbeam accelerometers," in *Tech. Dig. 8th Int. Conf. Solid-State Sensors and Actuators (Transducers'95)*, Stockholm, Sweden, June 1995, pp. 659–662.
[56] T. A. Roessig, R. T. Howe, A. P. Pisano, and J. H. Smith, "Surface micromachined resonant accelerometer," in *Tech. Dig. 9th Int. Conf. Solid-State Sensors and Actuators (Transducers'97)*, Chicago, IL, June 1997, pp. 859–862.
[57] Y. Omura, Y. Nonomura, and O. Tabata, "New resonant accelerometer based on a rigidity change," in *Tech. Dig. 9th Int. Conf. Solid-State Sensors and Actuators (Transducers'97)*, Chicago, IL, June 1997, pp. 855–858.
[58] R. Hiratsuka, D. C. van Duyn, T. Otraedian, and P. de Vries, "A novel accelerometer based on a silicon thermopile," in *Tech. Dig. 6th Int. Conf. Solid-State Sensors and Actuators (Transducers'91)*, San Francisco, CA, June 1991, pp. 420–423.
[59] A. M. Leung, J. Jones, E. Czyzewska, J. Chen, and B. Woods, "Micromachined accelerometer based on convection heat transfer," in *Proc. IEEE Micro Electro Mechanical Systems Workshop (MEMS'98)*, Heidelberg, Germany, Jan. 1998, pp. 627–630.
[60] D. Uttamchandani, D. Liang, and B. Culshaw, "A micromachined silicon accelerometer with fiber optic integration," in *Proc. SPIE Integrated Optics and Microstructures*, 1992, pp. 27–33.
[61] R. S. Huang, E. Abbaspour-Sani, and C. Y. Kwok, "A novel accelerometer using silicon micromachined cantilever supported optical grid and PIN photodetector," in *Tech. Dig. 8th Int. Conf. Solid-State Sensors and Actuators (Transducers'95)*, Stockholm, Sweden, June 1995, pp. 663–666.
[62] E. Abbaspour-Sani, R. S. Huang, and C. Y. Kwok, "A linear electromagnetic accelerometer," *Sensors Actuators A*, vol. 44, pp. 103–109, 1994.
[63] P. Chen, R. S. Muller, R. D. Jolly, G. L. Halac, R. M. White, A. P. Andrews, T. C. Lim, and M. E. Motamedi, "Integrated silicon microbeam PI-FET accelerometer," *IEEE Trans. Electron Devices*, vol. ED-29, pp. 363–369, Jan. 1982.
[64] D. L. DeVoe and A. P. Pisano, "A fully surface-micromachined piezoelectric accelerometer," in *Tech. Dig. 9th Int. Conf. Solid-State Sensors and Actuators (Transducers'97)*, Chicago, IL, June 1997, pp. 1205–1208.
[65] W. D. Frobenius, S. Zeitman, M. H. White, D. A. O'Sullivan, and R. G. Hamel, "Microminiature ganged threshold accelerometers compatible with integrated circuit technology," *IEEE Trans. Electron Devices*, vol. ED-19, pp. 37–40, Jan. 1972.
[66] J. Noetzel, T. Tonnesen, W. Benecke, J. Binder, and G. Mader, "Quasianalog accelerometer using microswitch array," in *Tech. Dig. 8th Int. Conf. Solid-State Sensors and Actuators (Transducers'95)*, Stockholm, Sweden, June 1995, pp. 671–674.
[67] A. Selvakumar, N. Yazdi, and K. Najafi, "A low power, wide range threshold acceleration sensing system," in *Proc. IEEE Micro Electro Mechanical Systems Workshop (MEMS'96)*, San Diego, CA, Feb. 1996, pp. 186–191.
[68] O. Kromer, O. Fromhein, H. Gemmeke, T. Kuhner, J. Mohr, and M. Strohramann, "High-precision readout circuit for LIGA acceleration sensors," *Sensors Actuators A*, vol. 46/47, pp. 196–200, 1995.
[69] A. Selvakumar, "A multifunctional silicon micromachining technology for high performance microsensors and microactuators," Ph.D. dissertation, University of Michigan, Ann Arbor, 1997.
[70] M. Offenberg, F. Larmer, B. Elsner, H. Munzel, and W. Riethmuller, "Novel process for a monolithic integrated accelerometer," in *Tech. Dig. 8th Int. Conf. Solid-State Sensors and Actuators (Transducers'95)*, Stockholm, Sweden, June 1995, pp. 589–592.
[71] "ADXL50-monolithic accelerometer with signal conditioning," Analog Devices, Norwood, MA, data sheet, 1993.
[72] E. Koen, F. Pourahmadi, and S. Terry, "A multilayer ceramic package for silicon micromachined accelerometers," in *Tech. Dig. 8th Int. Conf. Solid-State Sensors and Actuators (Transducers'95)*, Stockholm, Sweden, June 1995, pp. 273–276.
[73] M. L. Kniffin and M. Shah, "Packaging for silicon micromachined accelerometers," *Int. J. Microcircuits Electron. Packaging*, vol. 19, no. 1, pp. 75–86, 1996.
[74] W. M. Stalnaker, L. J. Spangler, G. S. Fehr, and G. Fujimoto, "Plastic SMD package technology for accelerometers," in *Proc. 1997 Int. Symp. Microelectronics*, Philadelphia, PA, Oct. 1997, pp. 197–202.
[75] R. P. van Kampen, M. J. Velekoop, P. M. Sarro, and R. F. Wolffenbuttel, "Application of electrostatic feedback to critical damping of an integrated silicon capacitive accelerometer," *Sensors Actuators A*, vol. 43, pp. 100–106, 1994.
[76] C. T. Nguyen, "Microelectromechanical resonators for oscillators and filters," in *Proc. 1995 IEEE Int. Ultrasonics Symp.*, 1995, pp. 489–499.
[77] M. S. Smith, L. Bowman, and J. D. Meindl, "Analysis, design, and performance of micropower circuits for a capacitive pressure sensor IC," *IEEE J. Solid-State Circuits*, vol. SC-21, pp. 1045–1056, Dec. 1986.
[78] C. Hierold, A. Hildebrandt, U. Naher, T. Scheiter, B. Mensching, M. Steger, and R Tielert, "A pure CMOS micromachined integrated accelerometer," in *Proc. IEEE Micro Electro Mechanical Systems Workshop (MEMS'96)*, San Diego, CA, 1996, pp. 174–179.
[79] Y. Matsumoto and M. Esashi, "Low drift integrated capacitive accelerometer with PLL servo techniques," in *Tech. Dig. 7th Int. Conf. Solid-State Sensors and Actuators (Transducers'93)*, Yokohama, Japan, June 1993, pp. 826–829.
[80] N. Yazdi, A. Mason, K. Najafi, and K. D. Wise, "A low-power interface circuit for capacitive sensors," in *Tech. Dig. Solid-State Sensor and Actuator Workshop*, Hilton Head Island, SC, June 1996, pp. 215–218.
[81] J. T. Kung, H. S. Lee, and R. T. Howe, "A digital readout technique for capacitive sensor applications," *IEEE J. Solid-State Circuits*, vol. 23, pp. 972–977, Aug. 1988.
[82] H. Leuthold and F. Rudolf, "An ASIC for high-resolution capacitive microaccelerometers," *Sensors Actuators*, vol. A21/A23, pp. 278–281, 1990.
[83] S. Suzuki and S. Tuchitani, "Semiconductor capacitance-type accelerometer with PWM electrostatic servo technique," *Sensors Actuators*, vol. A21/A23, pp. 316–319, 1990.
[84] "MMAS40G10D-micromachined accelerometer," Motorola, Phoenix, AZ, data sheet, 1997.
[85] "Dynamic measurement short form catalog," Endevco, San Juan Capistrano, CA, data sheet, 1997.
[86] "MS6100-low power accelerometer," CSEM, Neuchatel, Switzerland, data sheet, 1997.
[87] H. Lefevre, *The Fiber-Optic Gyroscope*. Norwood, MA: Artech House, 1993.
[88] A. Lawrence, *Modern Inertial Technology: Navigation, Guidance, and Control*. New York: Springer-Verlag, 1993.
[89] M. W. Putty and K. Najafi, "A micromachined vibrating ring gyroscope," in *Tech. Dig. Solid-State Sensor and Actuator Workshop*, Hilton Head Island, SC, June 1994, pp. 213–220.
[90] R. R. Ragan and D. D. Lynch, "Inertial technology for the future, Part X: Hemispherical resonator gyro," *IEEE Trans. Aerosp. Electron. Syst.*, vol. AES-20, p. 432, July 1984.
[91] J. Bernstein, S. Cho, A. T. King, A. Kourepenis, P. Maciel, and M. Weinberg, "A micromachined comb-drive tuning fork rate gyroscope," in *Proc. IEEE Micro Electro Mechanical Systems Workshop (MEMS'93)*, Fort Lauderdale, FL, Feb. 1993, pp. 143–148.
[92] M. Hashimoto, C. Cabuz, K. Minami, and M. Esashi, "Silicon resonant angular rate sensor using electromagnetic excitation and capacitive detection," *J. Micromech. Microeng.*, pp. 219–225, 1995.
[93] M. Lutz, W. Golderer, J. Gerstenmeier, J. Marek, B. Maihofer, S. Mahler, H. Munzel, and U. Bischof, "A precision yaw rate sensor in silicon micromachining," in *Tech. Dig. 9th Int. Conf. Solid-State Sensors and Actuators (Transducers'97)*, Chicago, IL, June 1997, pp. 847–850.
[94] R. Voss, K. Bauer, W. Ficker, T. Gleissner, W. Kupke, M. Rose, S. Sassen, J. Schalk, H. Seidel, and E. Stenzel, "Silicon angular rate sensor for automotive applications with piezoelectric drive and piezoresistive read-out," in *Tech. Dig. 9th Int. Conf. Solid-State Sensors and Actuators (Transducers'97)*, Chicago, IL, June 1997, pp. 879–882.

[95] K. Maenaka and T. Shiozawa, "A study of silicon angular rate sensors using anisotropic etching technology," *Sensors Actuators A*, vol. 43, pp. 72–77, 1994.
[96] J. Soderkvist, "Design of a solid-state gyroscopic sensor made of quartz," *Sensors Actuators*, vol. A21/A23, pp. 293–296, 1990.
[97] ——, "Micromachined gyroscopes," *Sensors Actuators A*, vol. 43, pp. 65–71, 1994.
[98] S. D. Orlosky and H. D. Morris, "Quartz rotation (rate) sensor," in *Proc. Sensor Expo*, Cleveland, OH, 1994, pp. 171–177.
[99] J. S. Burdess and T. Wren, "The theory of a piezoelectric disc gyroscope," *IEEE Trans. Aerosp. Electron. Syst.*, vol. AES-22, pp. 410–418, July 1986.
[100] P. Greiff, B. Boxenhorn, T. King, and L. Niles, "Silicon monolithic micromechanical gyroscope," in *Tech. Dig. 6th Int. Conf. Solid-State Sensors and Actuators (Transducers'91)*, San Francisco, CA, June 1991, pp. 966–968.
[101] Y. Gianchandani and K. Najafi, "A bulk silicon dissolved wafer process for microelectromechanical systems," *J. Microelectromech. Syst.*, pp. 77–85, June 1992.
[102] W. C. Tang, M. G. Lin, and R. T. Howe, "Electrostatically balanced comb drive for controlled levitation," in *Tech. Dig. Solid-State Sensor and Actuator Workshop*, Hilton Head Island, SC, June 1990, pp. 23–27.
[103] M. Weinberg, J. Bernstein, S. Cho, A. T. King, A. Kourepenis, P. Ward, and J. Sohn, "A micromachined comb-drive tuning fork gyroscope for commercial applications," in *Proc. Sensor Expo*, Cleveland, OH, 1994, pp. 187–193.
[104] F. Paoletti, M. A. Gretillat, and N. F. de Rooij, "A silicon micromachined vibrating gyroscope with piezoresistive detection and electromagnetic excitation," in *Proc. IEEE Micro Electro Mechanical Systems Workshop (MEMS'96)*, San Diego, CA, 1996, pp. 162–167.
[105] J. Soderkvist, "Micromachined vibrating gyroscopes," in *Proc. SPIE 1996 Symp. Micromachining and Microfabrication*, Austin, TX, 1996, pp. 152–160.
[106] S. Shoji, H. Kikuchi, and H. Torigoe, "Anodic bonding below 180°C for packaging and assembling of MEMS using lithium alminosilicate-β-quartz glass-ceramic," in *Proc. IEEE Micro Electro Mechanical Systems Workshop (MEMS'97)*, Japan, 1997, pp. 482–487.
[107] K. Maenaka, T. Fujita, Y. Konishi, and M. Maeda, "Analysis of a highly sensitive silicon gyroscope with cantilever beam as vibrating mass," *Sensors Actuators A*, vol. 54, pp. 568–573, 1996.
[108] D. Wood, G. Cooper, J. Burdess, A. Harris, and J. Cruickshank, "A silicon membrane gyroscope with electrostatic actuation and sensing," in *Proc. SPIE 1995 Symp. Micromachining and Microfabrication*, Austin, TX, 1995, pp. 74–83.
[109] H. Kuisma, T. Ryhanen, J. Lahdenpera, E. Punkka, S. Ruotsalainen, T. Sillanpaa, and H. Seppa, "A bulk micromachined silicon angular rate sensor," in *Tech. Dig. 9th Int. Conf. Solid-State Sensors and Actuators (Transducers'97)*, Chicago, IL, June 1997, pp. 875–878.
[110] W. A. Clark, R. T. Howe, and R. Horowitz, "Surface micromachined z-axis vibratory rate gyroscope," in *Tech. Dig. Solid-State Sensor and Actuator Workshop*, Hilton Head Island, SC, June 1996, pp. 283–287.
[111] T. Juneau and A. P. Pisano, "Micromachined dual input axis angular rate sensor," in *Tech. Dig. Solid-State Sensor & Actuator Workshop*, Hilton Head Island, SC, June 1996, pp. 299–302.
[112] Y. Oh, B. Lee, S. Baek, H. Kim, J. Kim, S. Kang, and C. Song, "A surface-micromachined tunable vibratory gyroscope," in *Proc. IEEE Micro Electro Mechanical Systems Workshop (MEMS'97)*, Japan, 1997, pp. 272–277.
[113] K. Y. Park, C. W. Lee, Y. S. Oh, and Y. H. Cho, "Laterally oscillated and force-balanced micro vibratory rate gyroscope supported by fish hook shape springs," in *Proc. IEEE Micro Electro Mechanical Systems Workshop (MEMS'97)*, Japan, 1997, pp. 494–499.
[114] S. An, Y. S. Oh, B. L. Lee, K. Y. Park, S. J. Kang, S. O. Choi, Y. I. Go, and C. M. Song, "Dual-axis microgyroscope with closed-loop detection," in *Proc. IEEE Micro Electro Mechanical Systems Workshop (MEMS'98)*, Heidelberg, Germany, Feb. 1998, pp. 328–333.
[115] K. Tanaka, Y. Mochida, M. Sugimoto, K. Moriya, T. Hasegawa, K. Atsuchi, and K. Ohwada, "A micromachined vibrating gyroscope," *Sensors Actuators A*, vol. 50, pp. 111–115, 1995.
[116] T. Juneau, A. P. Pisano, and J. H. Smith, "Dual axis operation of a micromachined rate gyroscope," in *Tech. Dig. 9th Int. Conf. Solid-State Sensors and Actuators (Transducers'97)*, Chicago, IL, June 1997, pp. 883–886.
[117] T. Fujita, T. Mizuno, R. Kenny, M. Maenaka, and M. Maeda, "Two-dimensional micromachined gyroscope," in *Tech. Dig. 9th Int. Conf. Solid-State Sensors and Actuators (Transducers'97)*, Chicago, IL, June 1997, pp. 887–890.
[118] T. K. Tang, R. C. Gutierrez, J. Z. Wilcox, C. Stell, V. Vorperian, R. Calvet, W. J Li, I. Charkaborty, R. Bartman, and W. J. Kaiser, "Silicon bulk micromachined vibratory gyroscope," in *Tech. Dig. Solid-State Sensor and Actuator Workshop*, Hilton Head Island, SC, June 1996, pp. 288–293.
[119] T. K. Tang, R. C. Gutierrez, C. B. Stell, V. Vorperian, G. A. Arakaki, J. T. Rice, W. J. Li, I. Chakraborty, K. Shcheglov, J. Z. Wilcox, and W. J. Kaiser, "A packaged silicon MEMS vibratory gyroscope for microspacecraft," in *Proc. IEEE Micro Electro Mechanical Systems Workshop (MEMS'97)*, Japan, 1997, pp. 500–505.
[120] W. Geiger, B. Folkmer, J. Merz, H. Sandmaier, and W. Lang, "A new silicon rate gyroscope," in *Proc. IEEE Micro Electro Mechanical Systems Workshop (MEMS'98)*, Heidelberg, Germany, Feb. 1998, pp. 615–620.
[121] M. W. Putty, "A micromachined vibrating ring gyroscope," Ph.D. dissertation, Univ. Michigan, Ann Arbor, Mar. 1995.
[122] D. R. Sparks, S. R. Zarabadi, J. D. Johnson, Q. Jiang, M. Chia, O. Larsen, W. Higdon, and P. Castillo-Borelley, "A CMOS integrated surface micromachined angular rate sensor: It's automotive applications," in *Tech. Dig. 9th Int. Conf. Solid-State Sensors and Actuators (Transducers'97)*, Chicago, IL, June 1997, pp. 851–854.
[123] F. Ayazi and K. Najafi, "Design and fabrication of a high-performance polysilicon vibrating ring gyroscope," in *Proc. IEEE Micro Electro Mechanical Systems Workshop (MEMS'98)*, Heidelberg, Germany, Feb. 1998, pp. 621–626.
[124] A. Selvakumar and K. Najafi, "High density vertical comb array microactuators fabricated using a novel bulk/poly-silicon trench refill technology," in *Tech. Dig. Solid-State Sensor and Actuator Workshop*, Hilton Head Island, SC, USA, 1994, pp. 138–141.
[125] I. Hopkin, "Performance and design of a silicon micromachined gyro," in *Proc. Symp. Gyro Technology*, Stuttgart, Germany, 1997, pp. 1.0–1.10.
[126] R. Torti, V. Gondhalekar, H. Tran, B. Selfors, S. Bart, and B. Maxwell, "Electrostatically suspended and sensed micromechanical rate gyroscope," in *Proc. SPIE 1994 Symp. on Micromachining and Microfabrication*, Austin, TX, 1994, pp. 27–31.
[127] C. Shearwood, C. B. Williams, P. H. Mellor, R. B. Yates, M. R. J. Gibbs, and A. D. Mattingley, "Levitation of a micromachined rotor for application in a rotating gyroscope," *Electron. Lett.*, vol. 31, no. 21, p. 1845, Oct. 1995.
[128] J. Soderkvist, "Piezoelectric beams and vibrating angular rate sensors," *IEEE Trans. Ultrason., Ferroelect., Frequency Contr.*, vol. 38, pp. 271–280, May 1991.
[129] S. T. Cho and F. M. Erdmann, "An on-chip hermetic packaging technology for micromechanical devices," in *Tech. Dig. Solid-State Sensor and Actuator Workshop*, Hilton Head, SC, June 1998.
[130] B. E. Boser, "Electronics for micromachined inertial sensors," in *Tech. Dig. 9th Int. Conf. Solid-State Sensors and Actuators (Transducers'97)*, Chicago, IL, USA, June 1997, pp. 1169–1172.
[131] S. R. Zarabadi, P. E. Castillo-Borelly, and J. D. Johnson, "An angular rate sensor interface IC," in *Dig. IEEE Custom Integrated Circuits Conf.*, 1996, pp. 311–314.
[132] C. Song, "Commercial vision of silicon based inertial sensors," in *Tech. Dig. 9th Int. Conf. Solid-State Sensors and Actuators (Transducers'97)*, Chicago, IL, June 1997, pp. 839–842.
[133] M. Weinberg, J. Bernstein, J. Borenstein, J. Campbell, J. Cousens, B. Cunningham, R. Fields, P. Greiff, B. Hugh, L. Niles, and J. Sohn, "Micromachining inertial instruments," in *Proc. SPIE 1996 Symp. Micromachining and Microfabrication*, Austin, TX, 1996.

Navid Yazdi received the B.S. degree (with Honors) from the University of Tehran, Iran, in 1988 and the M.S. degree from the University of Windsor, Windsor, Canada, in 1993, both in electrical engineering. He currently is pursuing the Ph.D. degree in electrical engineering at the University of Michigan, Ann Arbor.

From 1988 to 1991, he was an R&D Engineer at the University of Tehran, where he worked on hardware/software development for computer numerical control machine tools and large data-acquisition systems. From 1991 to 1993, he worked on architectures and mixed-signal circuit design for very-large-scale-integration (VLSI) implementation of artificial neural networks at the University of Windsor. Since 1993, his research work at the University of Michigan has been focused on high-performance mixed-signal interface circuits for microsensors, high-precision microaccelerometer design and fabrication, electromechanical oversampled sigma-delta modulators, and wireless telemetry for microsystems. His research interests include mixed analog–digital VLSI circuits for sensor interfacing and telecommunication applications, integrated inertial sensors, low-power wireless smart microsystems, and technologies for microelectromechanical systems.

Mr. Yazdi is a member of Sigma Xi and Tau Beta Pi. He received a University of Michigan Rackham Predoctoral Fellowship for 1996–1997. He received the Outstanding Graduate Student Achievement Award in electrical engineering from the College of Engineering, University of Michigan, in 1998.

Farrokh Ayazi was born in Tehran, Iran, in 1972. He received the B.S. degree in electrical engineering (with Honors) from the University of Tehran in 1994 and the M.S. degree in electrical engineering from the University of Michigan, Ann Arbor, in 1997. He currently is pursuing the Ph.D. degree at the Center for Integrated Sensors and Circuits, University of Michigan.

His doctoral work involves the design and development of precision silicon micromachined gyroscopes and their interface circuits. He also has been involved in characterization and fabrication of silicon micromachined accelerometers and their interface circuits. During the summer of 1993, he was with Schlumberger, Abu Dhabi, United Arab Emirates, where he completed an extensive course on sensing and data-aquisition techniques.

Mr. Ayazi received a Rackham Predoctoral Fellowship from the University of Michigan for 1998–1999.

Khalil Najafi (Senior Member, IEEE) was born in 1958. He received the B.S., M.S., and Ph.D. degrees in electrical engineering from the Department of Electrical Engineering and Computer Science, University of Michigan, Ann Arbor, in 1980, 1981, and 1986, respectively.

He has been with the Center for Integrated Sensors and Circuits, Department of Electrical Engineering and Computer Science, University of Michigan, as a Research Fellow (1986–1988), Assistant Research Scientist (1988–1990), Assistant Professor (1990–1993), and Associate Professor (1993–present). His research interests include development of microfabrication and micromachining technologies for solid-state integrated sensors and microactuators, analog and digital integrated circuits, implantable microtelemetry systems and transducers for biomedical applications and wireless communication, technologies and structures for microelectromechanical systems and microstructures, hermetic packaging techniques for microtransducers, and low-power wireless sensing/actuating systems. He has been active in the field of solid-state sensors and actuators for 15 years and has been involved in several conferences and workshops dealing with solid-state sensors and actuators, including the International Electron Devices Meeting, the Hilton-Head Solid-State Sensors and Actuators Workshop, and the IEEE/ASME Micro Electromechanical Systems Workshop. He is an Associate Editor for the *Journal of Micromechanics and Microengineering*.

Dr. Najafi received a National Science Foundation Young Investigator Award from 1992 to 1997. He received the Beatrice Winner Award for Editorial Excellence at the 1986 International Solid-State Circuits Conference and the Paul Rappaport Award for coauthoring the Best Paper published in IEEE TRANSACTIONS ON ELECTRON DEVICES. In 1994, he received the University of Michigan's Henry Russel Award for outstanding achievement and scholarship. In 1993, he was selected by students in Electrical Engineering and Computer Science Department as the Professor of the Year. Dr. Najafi is the Editor for Solid-State Sensors for IEEE TRANSACTIONS ON ELECTRON DEVICES.